The Astrophysical Journal, 891:40 (18pp), 2020 March 1 https://doi.org/10.3847/1538-4357/ab6e6d

Detection of Fluorine in Hot Extreme Helium Stars

Anirban Bhowmick[1], Gajendra Pandey[1], and David L. Lambert[2]
[1] Indian Institute of Astrophysics, Koramangala, Bengaluru 560 034, India; anirban@iiap.res.in, pandey@iiap.res.in
[2] W.J. McDonald Observatory and Department of Astronomy, The University of Texas at Austin, Austin, TX 78712, USA; dll@astro.as.utexas.edu
Received 2019 December 25; accepted 2020 January 20; published 2020 March 2

Abstract

The main objective of this paper is to explore abundances of fluorine in hot extreme helium stars (EHes). Overabundance of fluorine is a characteristic feature for cool EHes and R Coronae Borealis stars and further enforces their close connection. For hot EHes this relationship with the cooler EHes, based on their fluorine abundance is unexplored. We present in this paper the first abundance estimates of fluorine determined from singly ionized fluorine lines (F II) for 10 hot EHe stars from optical spectra. Fluorine abundances were determined using the F II lines in two windows centered at 3505 Å and 3850 Å. Six of the 10 stars show significant enhancement of fluorine similar to the cool EHes. Two carbon-poor hot EHes show no signature of fluorine and have a significant low upper limit for the F abundance. These fluorine abundances are compared with the other elemental abundances observed in these stars, which provide an idea about the formation and evolution of these stars. The trends of fluorine with C, O, and Ne show that significant helium burning after a CO–He white dwarf merger can account for a majority of the observed abundances. Predictions from simulations of white dwarf mergers are discussed in light of the observed abundances.

Unified Astronomy Thesaurus concepts: Stellar abundances (1577); Chemically peculiar stars (226); Hydrogen deficient stars (769); Helium-rich stars (715)

1. Introduction

Extreme helium stars (EHes) are helium-rich, hydrogen-deficient A- and B-type supergiants having effective temperatures in the range of 8000–35,000 K. The observed surface compositions of these stars are similar to those of the cooler hydrogen-deficient stars, namely, the R Coronae Borealis (RCB) and hydrogen-deficient carbon (HdC) stars. Apart from sharing extreme hydrogen deficiency, EHe, RCB, and HdC stars also exhibit common peculiar aspects of their chemical compositions.

The two most notable peculiarities in the compositions of these H-deficient stars are (1) the extreme overabundance of ^{18}O in HdC and cool RCBs such that $^{18}O/^{16}O > 1$ (Clayton et al. 2007) and (2) a startling overabundance of F in RCBs and cool EHes such that F relative to Fe is enhanced by 800–8000 times (Pandey 2006; Pandey et al. 2008; Hema et al. 2017). It is now of great interest to determine, as seems plausible, whether these peculiarities extend to the hot EHes. This paper addresses the F abundance of the hot EHes.

EHes are rare in the Galaxy, and hot EHes are necessarily extremely rare. Jeffery et al. (1996) list 21 EHes in their catalog. An additional EHe was reported recently (Jeffery 2017). There are about 17 known hot EHes with effective temperatures hotter than about 14,000 K, the focus of this paper. Ten hot EHes are examined here. For the hot EHes, nothing is known about the two notable abundance anomalies of the H-deficient cool stars, that is, ^{18}O and F. Since the O isotopic abundances are determined from CO lines in the infrared spectrum and CO molecules cannot exist in the atmospheres of hot (or cool) EHes, the O isotopic abundances are unobtainable for EHes. (Isotopic wavelength shifts for O I and O II lines are negligible.) Fluorine abundances are, however, obtainable for EHes.

The chemical compositions derived from their observed spectra suggest a hydrogen-deficient atmosphere including material exposed to both H and He burning. Based on their observed surface compositions, two principal theories are in place to explain their origins: the "double-degenerate" (DD) model and the "final-flash" (FF) model. Based primarily on the fluorine, neon, ^{13}C, and ^{18}O abundances, a consensus is now emerging for the DD scenario; however, a small fraction may be produced by the FF scenario. The principal version of the DD model involves the merger of an He white dwarf with a more massive C–O white dwarf following the decay of their orbit (Iben & Tutukov 1984; Webbink 1984). Other mergers may involve two He white dwarfs. The second model, the FF model, refers to a late or final He shell flash in a post-asymptotic giant branch (AGB) star. In this model (Iben et al. 1983), the ignition of the helium shell in a post-AGB star, say, a cooling white dwarf, results in what is known as a late or very late thermal pulse (Herwig 2001).

Simulations predict that a CO–He white dwarf merger in the DD scenario may produce conditions for partial helium burning that results in production of ^{18}O via $^{14}N(\alpha, \gamma)^{18}F(\beta^{+}\nu)^{18}O$ and of ^{19}F, the sole stable isotope of F (Clayton et al. 2007). Hence, the knowledge of the fluorine abundance and its relation to the other abundant species found in these stars plays an important role in discovering the nucleosynthesis processes taking place during and following helium accretion onto the C–O or He white dwarf in the DD scenario.

If the suite of abundance peculiarities is seen to be common across the HdC, RCB, and EHe, primarily a sequence of increasing effective temperature, a common formation scenario would seem to be a likely scenario. As noted above, the ^{18}O anomaly cannot be investigated in EHes. The F anomaly is determinable across the sequence. For warm RCBs and the cooler EHes, neutral fluorine (F I) lines have provided the high F overabundances (Pandey 2006; Pandey et al. 2008; Hema et al. 2017). For hot EHes, the F I lines are undetectable in optical spectra, but lines of ionized fluorine should be present in ultraviolet (3500–3900 Å) spectra if the F abundance is anomalous. To date, the only confirmed detection of F II lines in a H-deficient star is Pandey et al. (2014)'s detection of F II

Table 1
Log of Observations of the EHe Stars

Star Name	Date of Observation	Exposure time(seconds)	*V*-mag	S/N (3500 Å)	S/N(3800 Å)	Source of spectra	$R = \lambda/\Delta\lambda$
LS IV+6° 2	2006 Mar 31	2000	12.2	120		UVES	40000
	2006 Apr 21	2980	12.2		175	FEROS	45000
V652 Her	2005 Mar 1	600	10.5		110	FEROS	45000
	2017 Jun 4	2700(5)	10.5		65	HESP	28000
	2018 Apr 22	2700(3)	10.5		40	HESP	28000
DY Cen	2010 Feb 27	1800	12.5	140	120	UVES	40000
V2205 Oph	2005 Feb 26	600	10.5		100	FEROS	45000
	2017 Jun 4	2400(4)	10.5		60	HESP	28000
	2018 May 9	2400(3)	10.5		50	HESP	29000
	2018 May 10	2400(3)	10.5		38	HESP	29000
HD 144941	2006 Apr 10	780	10.1	270		UVES	40000
	2006 Jan 8	3000	10.1		250	FEROS	45000
LSE 78	2006 Jan 10	1500	11.2	155		UVES	40000
	2006 Apr 9	2400	11.2		170	FEROS	45000
BD +10° 2179	2006 May 10	1000	10.0	220		UVES	40000
	2006 Apr 12	2820	10.0		210	FEROS	45000
	2018 Jan 13	2400(3)	10.0		95	HESP	29000
	2018 Feb 10	2400(3)	10.0		110	HESP	29000
	2018 Mar 27	2400(3)	10.0		80	HESP	29000
V1920 Cyg	1996 Jul 25	1800	10.3		110	McDonald	48000
HD 124448	2006 Apr 10	975	10.0	190		UVES	40000
	2006 Apr 8	2820	10.0		200	FEROS	45000
PV Tel	2006 Apr 8	1500	9.3		180	FEROS	45000

lines at 3500–3510 Å in a spectrum of the hot EHe/hot RCB DY Cen. However, DY Cen is an odd H-deficient star in that it has a relatively high hydrogen abundance. Detection of fluorine in other hot EHes has yet to be explored. Here we report F abundances (or upper limits) for 10 hot EHes.

The paper is organized as follows: Section 2 discusses the observations, Section 3 addresses the identification of the F II lines, and Section 4 presents the abundance analysis and discusses the relations between the F and some other elemental abundances. Section 5 discusses the compositions of the hot EHes and other H-deficient stars in the light of predictions from simulations of the DD scenario. Section 6 concludes the paper with a few final remarks.

2. Observations

High-resolution optical echelle spectra of 10 hot EHes come from Himalayana Chandra Telescope (HCT)–HESP, ESO–FEROS, ESO–UVES, and the McDonald Observatory, as discussed below. All but two stars (DY Cen and V1920 Cyg) were observed with more than one telescope/spectrograph combination (see Table 1).

We observed three hot EHes, V652 Her, V2205 Oph, and BD +10° 2179, using the Hanle Echelle Spectrograph (HESP) (Sriram et al. 2018) mounted on the 2 m HCT at the Indian Astronomical Observatory (IAO) in Hanle, Ladakh, India, during 2017 and 2018 to look specifically for F II lines in the 3500 Å and 3800 Å regions. The observing details are shown in Table 1. A Th-Ar lamp was observed for wavelength calibration. To normalize the pixel-to-pixel variation in the sensitivity of the CCD, many exposures known as flat frames with differing spectrograph focus (in focus and out of focus) were obtained using a featureless quartz-halogen lamp. All the flat frames were combined to create a master flat with very high signal for flat correction. A spectrum of a rapidly rotating B-type bright star was obtained during each observing run for aperture extraction of faint program stars and also for removing the atmospheric lines. The data were reduced using standard IRAF[3] packages for bias correction, flat correction, aperture extraction, and wavelength calibration. The final wavelength-calibrated spectra of these three stars, V652 Her, V2205 Oph, and BD +10° 2179, were combined (see below) with spectra from the ESO Data Archives.

Table 2
Details of the Spectra

Star name	Wavelength Window			
	3505 Å		3850 Å	
	S/N	$R(\lambda/\Delta\lambda)$	S/N	$R(\lambda/\Delta\lambda)$
LS IV+6° 2	225	35000	260	37500
V652 Her	⋯	⋯	175	26000
DY Cen	160	33000	210	31000
V2205 Oph	⋯	⋯	320	27000
HD 144941	370	38000	340	37000
LSE 78	280	36000	220	36000
BD +10° 2179	320	38000	280	28000
V1920 Cyg	⋯	⋯	140	30000
HD 124448	220	39000	240	37500
PV Tel	⋯	⋯	220	38000

We also retrieved high-resolution optical spectra of 10 hot EHes from the European Southern Observatory (ESO) Data Archives.[4] These observations were made with ESO Telescopes at the La Silla and the Paranal Observatory under program IDs 077.D–0458, 284.D–5048, and 074B–0455. The spectra were recorded using FEROS on the ESO 2.2 m telescope in La Silla,

[3] IRAF is distributed by the National Optical Astronomy Observatory, which is operated by the Association of Universities for Research in Astronomy under a cooperative agreement with the National Science Foundation.
[4] http://archive.eso.org/wdb/wdb/adp/phase3_main/form

Table 3
F II Lines from $3s - 3p$ and $3p - 3d$ Transition Array Contributing to the Spectra of the Analyzed Stars

Multiplet No.	λ Å	χ (ev)	log *gf*	Likely Contributors
1	**3847.086**	21.88	0.31	F II, N II λ 3847.38
	3849.986	21.88	0.16	F II, Mg II(weak) λ 3850.40
	3851.667	21.88	−0.06	F II, O II λ 3851.47
2	4024.727	22.67	0.16	F II, He I, λ 4023.986, 4026.189, 4026.362 (very strong)
	4025.010	22.67	−0.54	F II, He I, λ 4023.986, 4026.189, 4026.362 (very strong)
	4025.495	22.67	−0.06	F II, He I, λ 4023.986, 4026.189, 4026.362 (very strong)
3	**3505.614**	25.10	0.676	F II
	3505.520	25.10	0.09	F II
	3505.370	25.10	−0.757	F II
	3503.095	25.10	0.391	F II, Ne II λ 3503.61
	3502.954	25.10	0.187	F II, He I λ 3502.393 (strong)
	3501.416	25.10	0.074	F II, He I λ 3498.659 (very strong), Fe III λ 3501.767
4	4103.525	25.75	0.559	F II, O II λ 4103.017, N III λ 4103.37 (strong)
	4103.085	25.75	0.289	F II, O II λ 4103.017, N III λ 4103.37 (strong)
	4103.724	25.75	−0.064	F II, N III λ 4103.37 (strong)
	4103.871	25.75	−0.19	F II N III λ 4103.37 (strong)
5	4109.173	26.26	0.45	F II, O II λ 4108.75, Mg II, λ 4109.54
	4116.547	26.27	0.18	F II, Si IV λ 4116.104 (strong)
	4119.219	26.27	−0.01	F II, O II λ 4119.221 (strong)

Notes.
The F II lines used in abundance determinations are shown in bold.

Chile, and UVES on the ESO Very Large Telescope at Paranal, Chile. The details are given in Table 1. FEROS provides the useful wavelength range of 3530–9200 Å, whereas the UVES provides spectra in the following wavelength windows: 3050–3870 Å, 3280–4560 Å, and 5655–9460 Å, 6650–8540 Å, and 8650–10240 Å.

The spectrum of the hot EHe star V1920 Cyg was observed using the W. J. McDonald Observatory's Harlan J. Smith 2.7 m telescope with the Robert G. Tull cross-dispersed echelle spectrograph during 1996 at a resolving power of about 30,000 (Tull et al. 1995). V1920 Cyg's spectrum is discussed in Pandey et al. (2006), and the relevant details are also provided in Table 1.

Spectra retrieved from archival data and those obtained from HESP were further smoothed to increase the signal-to-noise ratio. These spectra were finally normalized to continuum. Note that the spectra were smoothed to the limit that the stellar line profiles remain unaltered. To ensure this, the smoothed spectrum was compared with the unsmoothed one. The resolving power of the smoothed spectrum was determined by measuring the FWHM of telluric lines in the 6925 Å region. If telluric lines were not available for determining the spectral resolution of the smoothed spectra, the reported resolving power in the archives was used by taking into account the smoothening factor.

Frames with symmetric absorption line profiles and with minimum core emission were chosen for analysis; many EHes show variable spectra with radial velocity changes, variable line profiles, and even emission features. The spectra obtained from each individual frame were compared to check for the presence of any artifact. The signal in the spectra obtained through HESP was very low in the 3500 Å region, hence we have used only the spectral region above 3800 Å region for analysis. To further improve the signal-to-noise ratio, the spectrum from archival data and that from HESP, if available, were coadded for final analysis. Note that the observed spectra are brought to the rest wavelength using well-known stellar lines. The details of the final coadded spectra are given in Table 2.

3. Identification of F II Lines

Multiplets numbered 1–5 in the Revised Multiplet Table (RMT) of Moore (1972) and by Wiese et al. (1996) are the potential contributors of F II absorption lines to the spectra of hot EHe stars. A complete list of the transitions that includes their wavelengths, lower excitation potential, and log-*gf* values for lines of these multiplets was compiled from the NIST database.[5]

Four F II lines were identified as the main or significant contributors to stellar lines (see Table 3). These four lines consist of all three lines of muliplet 1, 3847.086 Å, 3849.986 Å, and 3851.667 Å, and the fourth line centered at 3505.614 Å of multiplet 3. Note that the F II line profile at 3505.614 Å, which appears as one, is a blend of three components 3505.614 Å 3505.52 Å, and 3505.37 Å (see Table 3). Lines at 3849.986 Å of multiplet 1 and 3505.614 Å of multiplet 3 are relatively free of blends and are best suited for determining the F abundance (see Table 3). All the lines of multiplets 1 and 3 are shown in Figures 1 and 2, where the spectra of hot EHes are ordered from top to bottom in order of decreasing effective temperature. The wavelength windows corresponding to Figures 1 and 2 are centered around 3508 Å and 3850 Å, respectively. Note that the spectra of V652 Her, V2205 Oph, and V1920 Cyg were not available or were very noisy in the window 3490–3520 Å. Also, for the other multiplets of F II lines, a thorough search was conducted for the blending lines, and strong blending of lines from other atomic species is noted (see Table 3). These multiplets were not selected for measuring the fluorine abundance: multiplet 2 is heavily blended with a Stark broadened strong He I line profile, and multiplets 4 and 5 are blended severely by lines of other elements. The blended lines were identified using the

[5] https://physics.nist.gov/PhysRefData/ASD/lines_form.html

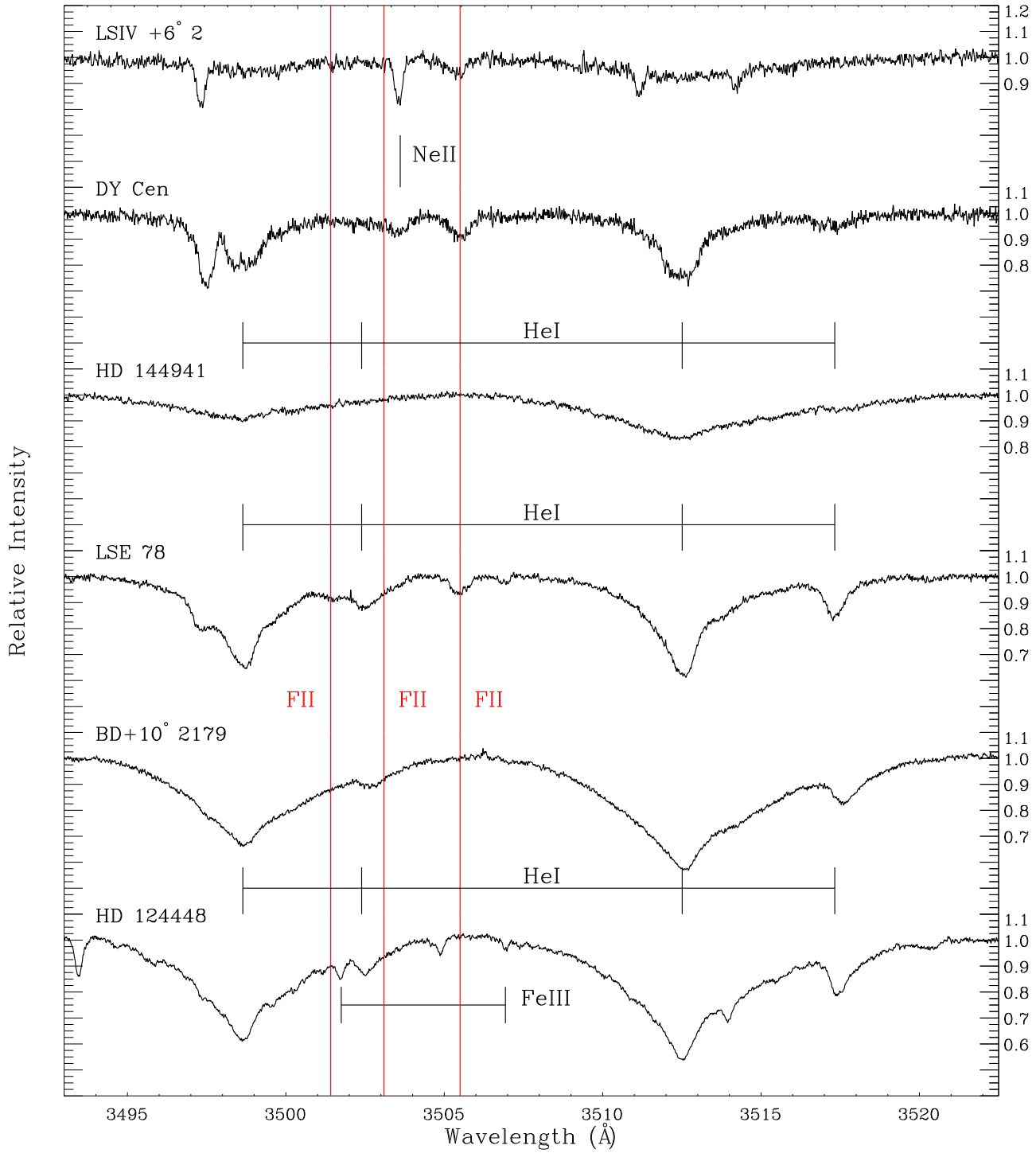

Figure 1. Comparison of the spectra with key identifications in the 3500 Å region. The stars are arranged according to their effective temperature, with hottest on the top and coolest at the bottom. The red lines represent the F II lines of Revised Multiplet Table (RMT) 3 in this window.

RMT (Moore 1972), tables of the spectra of H, C, N, and O (Moore 1993), and the NIST Atomic Spectra Database,[6] which also provides the line's *gf*-value.

4. Abundance Analysis

The abundance of an element X in normal stars is quoted with respect to hydrogen (i.e., X/H) due to hydrogen being the main contributor to the continuous opacity directly or indirectly as well as the most abundant element in their atmospheres. A measure of fractional abundance for the element X is also given by the mass fraction, $Z(X)$, where

$$Z(X) = \frac{\mu_X N_X}{\mu_H N_H + \mu_{\rm He} N_{\rm He} + ... + \mu_i N_i} = \frac{\mu_X N_X}{(\sum \mu_i N_i)} \quad (1)$$

$$\simeq \frac{\mu_X A_X}{1 + 4A_{\rm He}}, \quad (2)$$

[6] https://physics.nist.gov/PhysRefData/ASD/lines_form.html

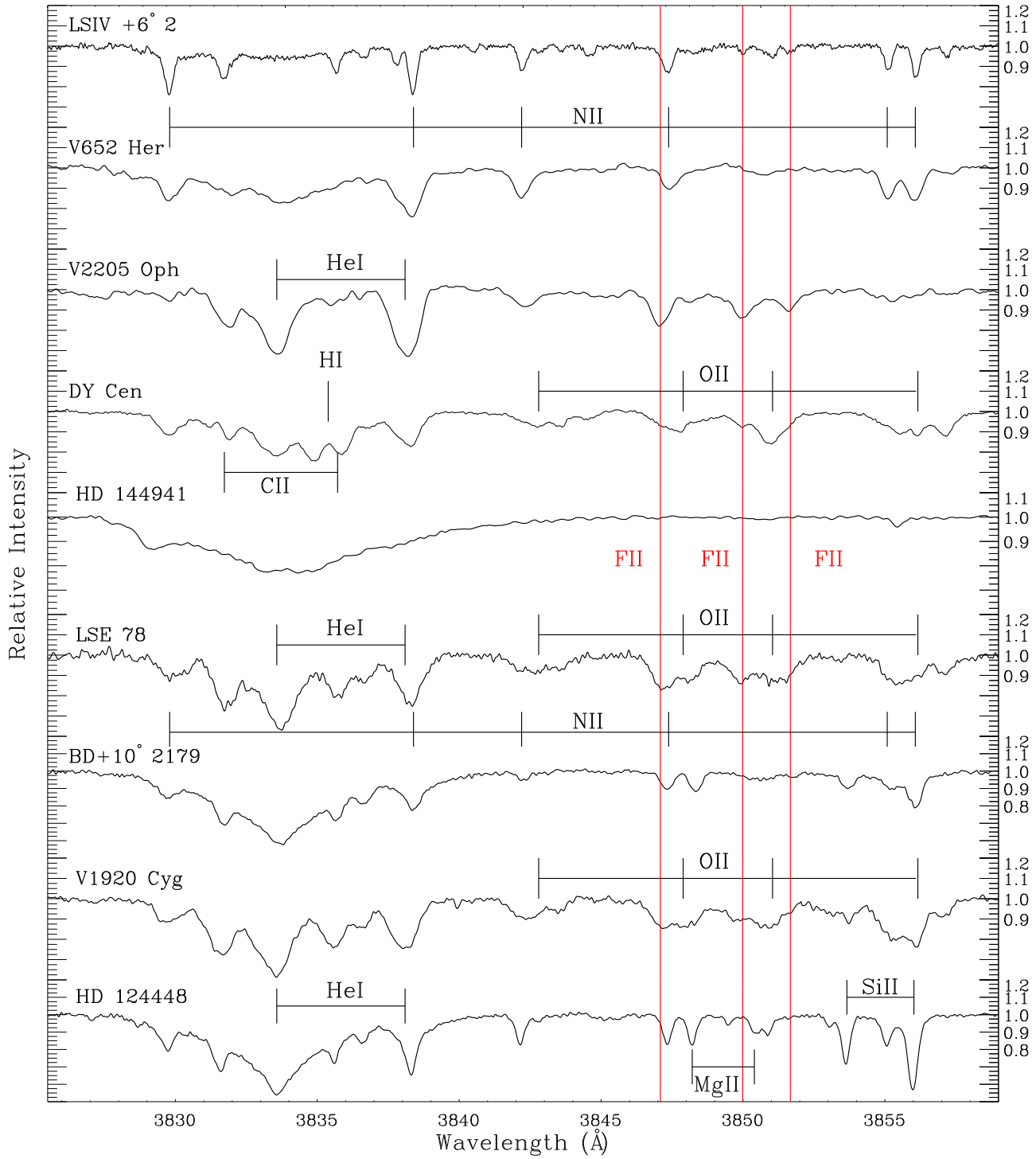

Figure 2. Comparison of the spectra with key identifications in the 3850 Å region. The stars are arranged according to their effective temperature, with hottest on the top and coolest at the bottom. The red lines represents the F II lines of RMT 1 in this window.

where μ_X is the atomic weight of element X and $A_X = X/\mathrm{H}$. Hence, $Z(X)$ is directly estimated from A_X, a result of abundance analysis of the observed spectrum, and an assumption about A_{He} if helium lines are not observable.

For the case of hydrogen-poor stars like the hot EHes, helium may be the main contributor to the continuum opacity directly or indirectly and also the most abundant element in their atmospheres, where the H/He ratio has been changed by the addition of nuclear-processed material from H- and He-burning layers. Thus, the abundance of an element X is determined with respect to helium, that is, $X/\mathrm{He} = A'_X$, and the Equation (1) reduces to

$$Z(X) = \frac{\mu_X A'_X}{H/\mathrm{He} + 4 + 12C/\mathrm{He} + ..\mu_i A'_i}. \quad (3)$$

Due to hydrogen being very poor in these stars, H/He is very small and like other trace elements can be ignored; then the

Table 4
Derived Abundances of Fluorine in Hot EHes

Star name	($T_{\rm eff}$, log g, ξ)	logϵ(F)						
		3847.086 Å	3849.986 Å	3851.667 Å	3505.614 Å	Mean	σ_1[a]	σ_2[b]
LS IV+6° 2	(32000, 4.20, 9.0)[c]	6.5	6.4	6.4	6.6	6.5	0.1	±0.1
V652 Her	(25300, 3.25, 13.0)[d]	<5.7	<5.5	<5.6	⋯	<5.6	⋯	⋯
V2205 Oph	(24800, 2.85, 23.0)[c]	7.0	7.0	7.0	⋯	7.0	0.1	±0.1
DY Cen	(24750, 2.65, 24.0)[f]	6.7	6.9	6.8	7.0	6.9	0.1	±0.2
HD 144941	(21000, 3.35, 10.0)[d]	<5.5	<5.7	<5.5	<5.5	<5.6	⋯	⋯
LSE 78	(18300, 2.2, 16.0)[f]	7.4	7.4	7.4	7.3	7.4	0.1	±0.2
BD +10° 2179	(17000, 2.6, 7.5)[e]	6.4	6.5	6.4	<6.5	6.4	0.2	±0.1
V1920 Cyg	(16300, 1.8, 20)[f]	7.5	7.6	7.5	⋯	7.5	0.2	±0.1
HD 124448	(15500, 2.0, 12)[f]	<6.0	<6.0	<6.0	<6.0	<6.0	⋯	⋯
PV Tel	(13750, 1.6, 25.0)[c]	<6.5	<6.5	<6.5	⋯	<6.5	⋯	⋯

Notes.
[a] rms error: $\Delta T_{\rm eff} = \pm 500$K, $\Delta \log g = \pm 0.2$ cgs.
[b] rms error: line-to-line scatter.
[c] (Pandey & Lambert 2011).
[d] (Pandey & Lambert 2017).
[e] (Pandey et al. 2014).
[f] (Pandey et al. 2006).

Table 5
Elemental Abundances of Hot EHes

Star name	log$\epsilon(X)$							Ref
	C	N	O	Ne	F	Fe	Zr	
LS IV+6° 2	9.4	8.3	8.2	8.7	6.5	7.1	⋯	P11[a]
V652 Her	7.0	8.7	7.6	8.1	⩽5.6	7.1	⋯	P17[b]
V2205 Oph	9.1	7.8	8.0	8.2	7.0	6.6	⋯	P11[a]
DY Cen	9.6	7.8	9.0	8.0	6.9	6.0	⋯	P14[c]
HD 144941	6.9	6.4	7.1	7.2	⩽5.6	⩽6.6	⋯	P17[b]
LSE 78	9.4	8.3	9.4	8.7	7.4	6.8	3.5	P11[a]; P06a[d]
BD +10° 2179	9.3	8.1	7.9	7.9	6.4	6.2	⩽2.6	P11[a]; P06a[d]
V1920 Cyg	9.6	8.6	9.9	8.5	7.5	6.8	3.7	P11[a]; P06a[d]
HD 124448	9.1	8.7	8.3	7.7	⩽6.0	7.2	2.7	P11[a]; P06a[d]
PV Tel	9.2	8.6	8.8	7.6	⩽6.5	7.0	3.1	P11[a]; P06a[d]

Notes.
[a] (Pandey & Lambert 2011).
[b] (Pandey & Lambert 2017).
[c] (Pandey et al. 2014).
[d] (Pandey et al. 2006).

above equation reduces to

$$Z(X) \simeq \frac{\mu_X A_X^{'}}{4 + 12C/\mathrm{He}}. \quad (4)$$

The C/He can be spectroscopically determined for hot EHes (≃0.01), and the abundance of any element X for a hot hydrogen-deficient star like hot EHes can be directly measured spectroscopically, that is, $A_X^{'} = X/\mathrm{He}$.

Due to the conservation of nucleons during different stages of nuclear burning, the derived abundances are normalized based on the convention that $\log \epsilon(X) = \log(X/\mathrm{H}) + 12.0$ to a scale in which $\log \sum \mu_i \epsilon(i) = 12.15$, where 12.15 is determined from solar abundances with He/H ≃ 0.1. Based on this normalization convention, and considering X/He as the measure of abundance of an element X in hot H-poor or hot EHe stars, the helium abundance log ϵ(He) is about 11.54 from Equation (4).

The F abundance is derived from the four best F II lines (Table 3). Since these lines are subject to blending, spectrum synthesis was used to locate a F II line's contribution. The code SYNSPEC (Hubeny et al. 1994) was used with the LTE model atmospheres of individual stars (see Table 4) from Pandey et al. (2006, 2014) and Pandey & Lambert (2011, 2017). Synthetic spectra were convolved with the instrumental profile and the broadening corresponding to the rotational velocity derived from weak and symmetric O II or N II lines in the star's spectrum. All the key lines were used to compose a line list for spectrum synthesis. Selected lines of several elements were synthesized. Derived LTE abundances are in fair agreement with those reported in our earlier abundance analyses (Pandey et al. 2006; Pandey & Lambert 2011; Pandey et al. 2014; Pandey & Lambert 2017). Adopted model atmospheres ($T_{\rm eff}$ = effective temperature, log g = surface gravity, ξ = microturbulence) and the F abundances from the individual F II lines and the line-to-line scatter are given in Table 4.

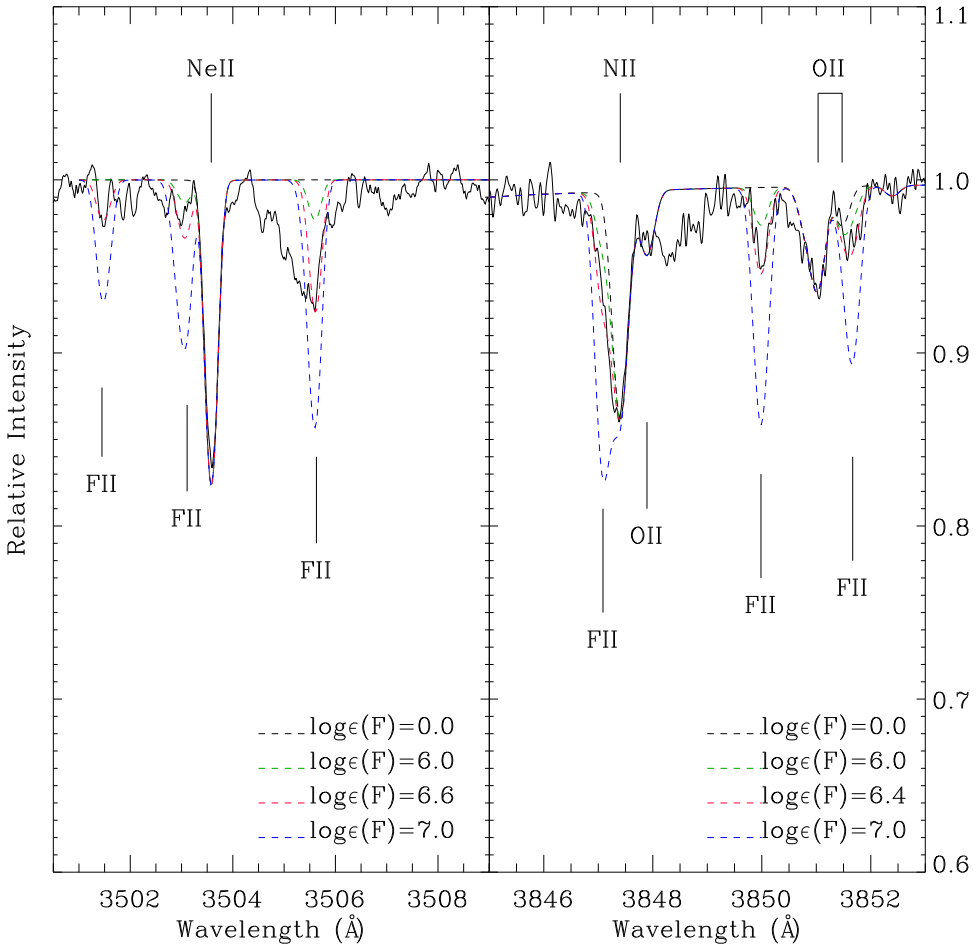

Figure 3. Observed F II in 3500 Å and 3850 Å of LS IV+6° 2 (solid line) with key lines marked. Synthetic spectra are shown for four fluorine abundances.

Abundances of other elements (C, N, O, Ne, Fe, and Zr) are given in Table 5.

The two spectral regions providing the F II lines are displayed in Figures 1 and 2 with the EHes arranged in order of decreasing effective temperature from top to bottom. By inspection, it is obvious that the F II lines do not vary smoothly with effective temperature; the F abundance can be greatly different in stars of similar effective temperature. Consider, for example, V652 Her and V2205 Oph in Figure 2 with the three F II lines prominent in the spectrum of V2205 Oph but seemingly absent from the spectrum of V652 Her. The two stars have similar atmospheric parameters but F abundances differing by at least 1.5 dex (Table 4).

Brief remarks follow on the spectrum syntheses of the F II lines in the individual stars and their F abundances beginning with the hottest star LS IV+6° 002. Observed and synthetic spectra are shown for each star.

LS IV+6° 002. The windows at 3505 Å and 3850 Å are both available for this star. The F abundance is based primarily on the lines at 3849.986 Å and 3851.7 Å with the two weakest lines at 3501.4 Å and 3503.1 Å providing supporting evidence as to the maximum F abundance allowed by these lines (Figure 3). The 3847.1 Å line in the blue wing of a strong N II line appears to be present, but assessment of its strength is dependent on the adopted width of the N II line. The 3505 Å blend of three RMT 3 lines appears to be present at the F abundance provided by other lines but is seriously blended with an unidentified line. The F abundance of $\log \epsilon(\mathrm{F}) = 6.5$ seems appropriate for this star.

V652 Her. Only the 3850 Å window is available. Spectrum synthesis does not provide convincing detection of a F II line (Figure 4). An upper limit of $\log \epsilon(\mathrm{F}) = 5.6$ is provided by each of the RMT 1 lines. This star is very clearly F poor relative to LS IV +6° 002 (and other F-rich stars).

V2205 Oph. The 3505 Å window is not available. In the 3850 Å window, the three RMT 1 F II lines are clearly present with a consistent abundance of $\log \epsilon(\mathrm{F}) = 7.0$ (Figure 5). Blending lines of N II and O II are pleasingly weak in this star, ensuring the consistency of the F abundance from the three lines.

DY Cen. Consistent F abundances are obtained from unblended or relatively unblended lines in both windows (Figure 6). The unblended 3505.5 Å line provides the F abundance of $\log \epsilon(\mathrm{F}) = 7$. The other two lines in the RMT 3 are possibly present and consistent with this abundance. In RMT 1, the blending by the N II and O II lines is much stronger than in V2205 Oph (Figure 5). The weaker two F II lines of this RMT provide a consistent F abundance, which is supported by the 3851.7 Å line now seriously blended with the O II line. An F abundance of $\log \epsilon(\mathrm{F}) = 6.9$ is recommended.

HD 144941. The wavelength regions centered at 3505 Å and 3850 Å are available and do not show detectable F II lines in the observed spectrum (see Figure 7). An upper limit of

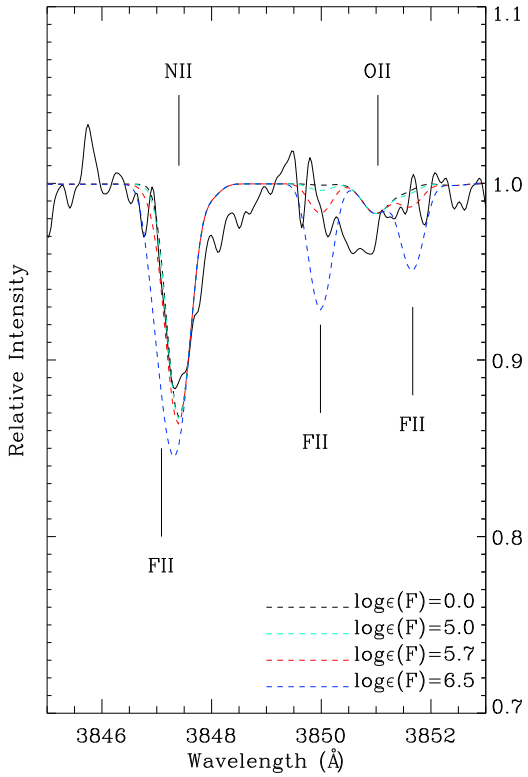

Figure 4. Observed F II in 3850 Å of V652 Her (solid line) with key lines marked. Synthetic spectra are shown for four fluorine abundances.

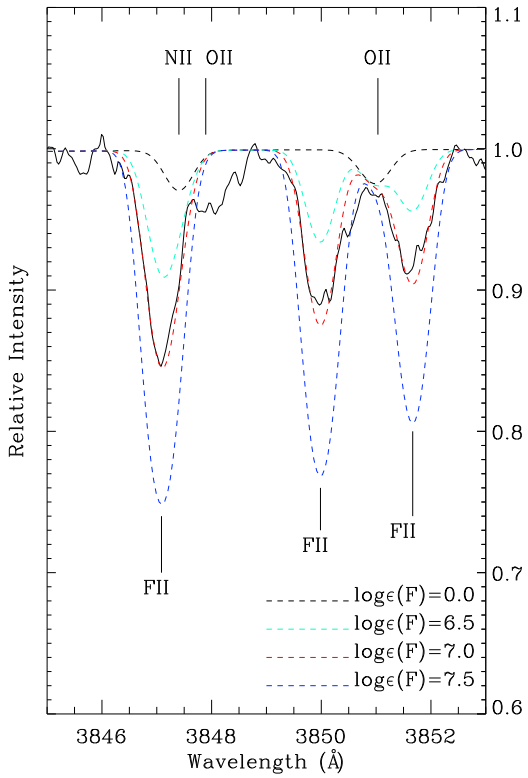

Figure 5. Observed F II in 3850 Å of V2205 Oph (solid line) with key lines marked. Synthetic spectra are shown for four fluorine abundances.

$\log \epsilon(\mathrm{F}) = 5.6$ is obtained by each of the RMT 1 and RMT 3 lines. This star is clearly very F poor and similar to the other carbon-poor hot EHe star V652 Her.

LSE 78. The F abundance is provided by the F II lines at 3505.5 Å from RMT 3 and the three lines of RMT 1. The F abundance of $\log \epsilon(\mathrm{F}) = 7.4$ reproduces these lines (Figure 8).

BD +10° 2179. In both the 3505 Å and 3850 Å windows, the F II lines are weak (Figure 9). The 3505.5 Å is not detected, and the abundance upper limit for F of $\log \epsilon(\mathrm{F}) = 6.5$ is set. In RMT 3, the cleanest line is at 3851.7 Å and gives the F abundance of about $\log \epsilon(\mathrm{F}) = 6.4$. The other two lines of this RMT are blended but confirm the abundance of 6.4.

V1920 Cyg. Only the 3850 Å window is available where the three F II lines are blended (Figure 10). The least blended line at 3850.0 Å gives the F abundance of $\log \epsilon(\mathrm{F}) = 7.5$, a value consistent with determinations from the two more seriously blended lines.

HD 124448. Both wavelength regions are available, but neither show evidence for the F II lines (Figure 11). The 3505.5 Å is clearly absent. In the 3850 Å window, blends are an issue, but the 3850.0 Å and 3851.7 Å lines are absent. An upper limit to the F abundance of $\log \epsilon(\mathrm{F}) = 6.0$ may be set.

PV Tel. Only the 3850 Å window is available (Figure 12). Spectrum synthesis does not provide convincing detection of an F II line. An upper limit of $\log \epsilon(\mathrm{F}) = 6.5$ is provided by the 3847.1 Å and 3851.7 Å lines.

Our previous investigations of the compositions of hot EHe stars included analyses of the Ne abundance from Ne I and/or Ne II lines. When both neutral and singly ionized lines were available, it was found that the Ne abundance from the neutral lines was higher than that from the singly ionized lines. For example, the LTE neon abundances obtained by Pandey & Lambert (2011) for V2205 Oph from Ne I lines were 0.8 dex higher than those obtained from Ne II lines. This difference arises from non-LTE effects principally affecting the Ne I lines, a suggestion thoroughly confirmed by a non-LTE study by Pandey & Lambert (2011). Noting that the atomic structure of the F atom and the detected F I lines are not dissimilar to the Ne atom and the non-LTE-affected Ne I lines, we attempted to set limits on the non-LTE effects on the F abundances by analyzing F I and F II lines in the same star.

In the present sample of hot EHes, examination of the spectrum of V1920 Cyg and LSE 78 led to the detection of the F I at the 6856.02 Å line (Figures 13 and 14) with the estimated F abundances of 7.8 and 7.5, respectively. This F I line at 6856.02 Å is the strongest F I line, and the weaker F I lines are consistent with it. The abundance difference between that from the F II and the F I lines is −0.3 and −0.1 dex for V1920 Cyg and LSE 78, respectively. These differences limit severely the non-LTE effects in the conditions prevailing in both V1920 Cyg and LSE 78. As a complementary effort, we have returned to spectra of the cooler EHes where the F abundance is based on the F I lines to look for F II lines. Two stars had effective temperatures sufficiently high, with the available spectra possessing adequate signal-to-noise ratio in the blue to provide interesting limits on F II lines: LSS 3378 and PV Tel. For LSS 3378, the F II lines from multiplet 1 provide the upper limit of 8.0, which is consistent with the determination of 7.3 from the F I lines, a comparison that provides no information on the non-LTE effects. For PV Tel, the F II lines set the upper limit 6.5, which is a significant improvement over the limit ($\leqslant$7.2) reported by Pandey (2006) from the F I lines. Other EHes where in the future one might get both F I and F II lines are LS IV −1° 002 and LSS 4357. A key point to note is that the level of the F overabundances in the EHes is around a factor

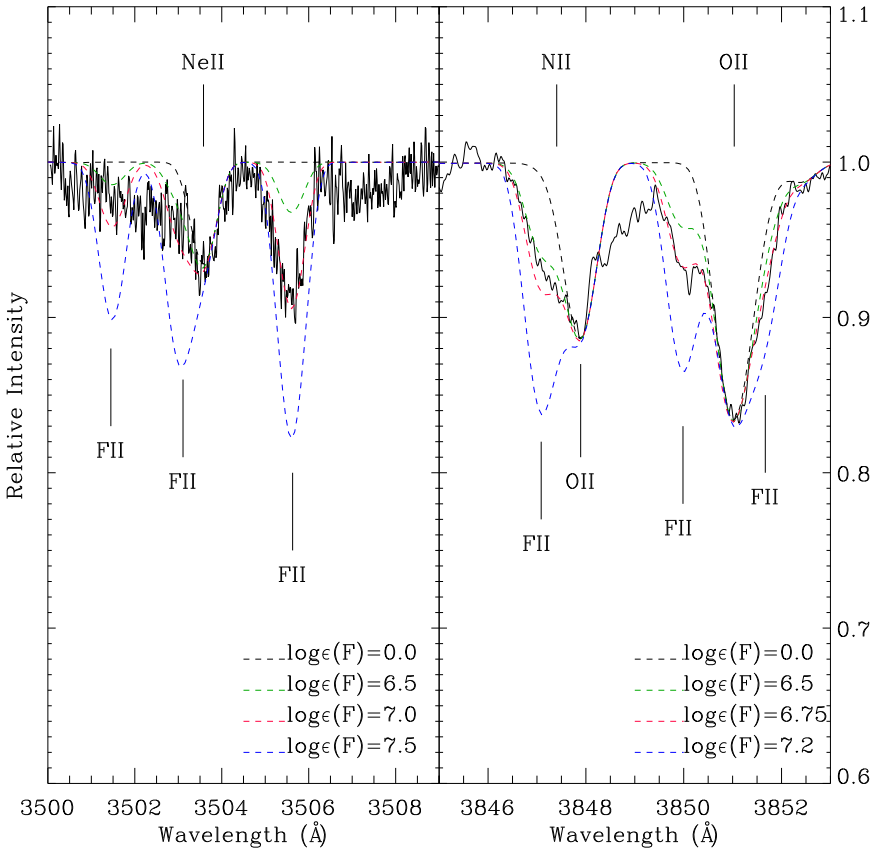

Figure 6. Observed F II in 3500 Å and 3850 Å of DY Cen (solid line) with key lines marked. Synthetic spectra are shown for four fluorine abundances.

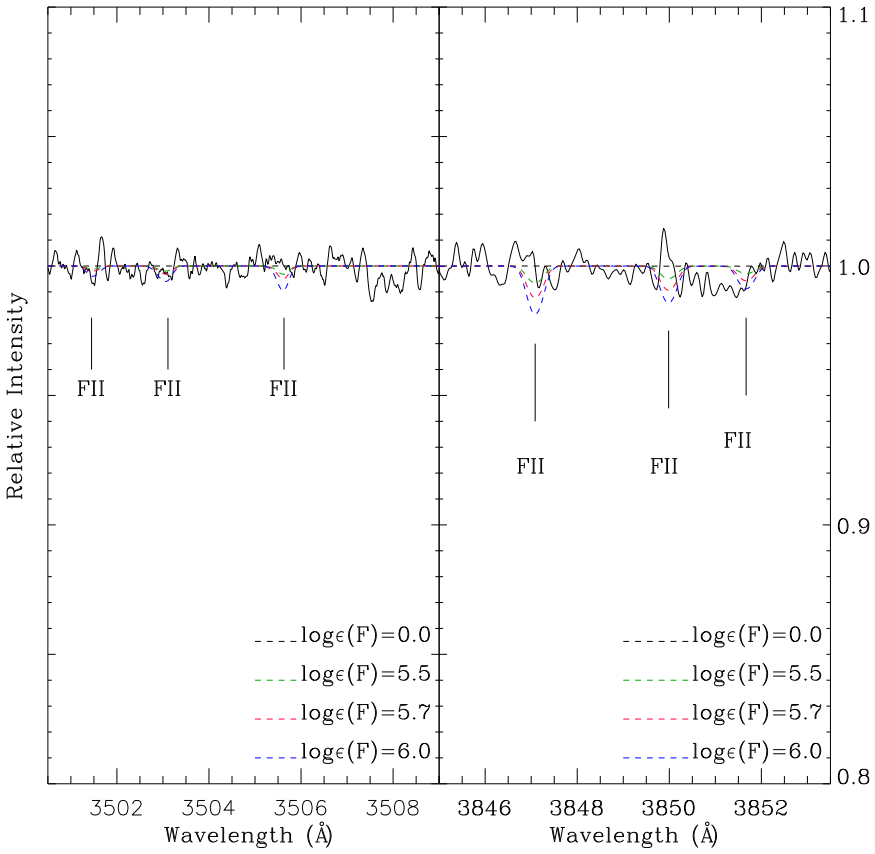

Figure 7. Observed F II in 3500 Å and 3850 Å of HD 144941 (solid line) with key lines marked. Synthetic spectra are shown for four fluorine abundances.

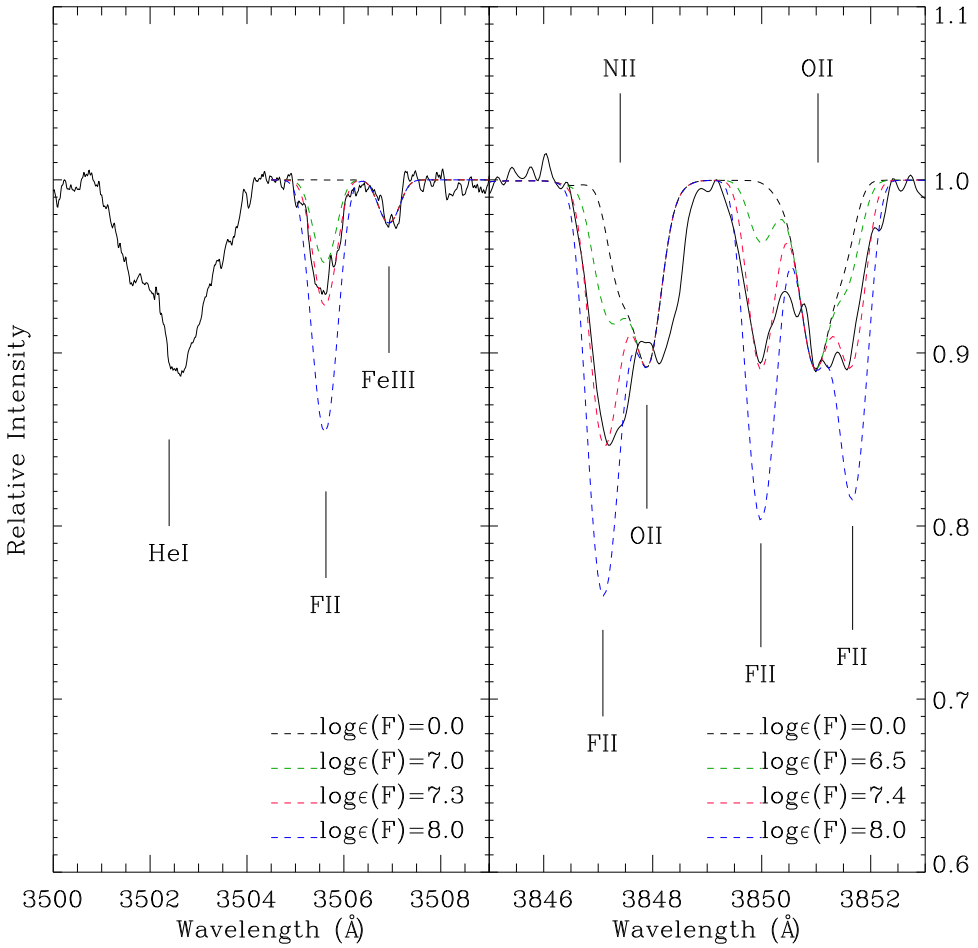

Figure 8. Observed F II in 3500 Å and 3850 Å of LSE 78 (solid line) with key lines marked. Synthetic spectra are shown for four fluorine abundances. Note that the He I line at 3502 Å in the left panel of the above figure is not synthesized due to unavailability of log-*gf* values in the NIST database.

of 1000 but the non-LTE effects, if comparable to those on the Ne I lines, are less than a factor of 10. Thus, a very significant overabundance of F in EHes and RCBs is not in doubt because of the present lack of non-LTE calculations for the fluorine atom.

4.1. Fluorine Enrichment

Fluorine abundances across the sample of 10 hot EHes, which range from 7.5 to an upper limit of 5.6, are shown in Figure 15 as a function of Fe abundance where the two C-poor stars (V652 Her and HD 144941) are distinguished. The F overabundance is remarkable. Fluorine abundances for the cool EHes (Pandey 2006) and the majority and minority RCBs (Pandey et al. 2008; Hema et al. 2017) are added to Figure 15. The spread of F abundances across the total sample of H-deficient stars far exceeds the errors of measurement. Figure 15 suggests that a few stars may have an F abundance much lower than the typical EHe and RCB. This minority includes the two C-poor hot EHe stars V652 Her and HD 144941, the minority RCB V854 Cen with $\log \epsilon(\mathrm{Fe}) = 5$, the majority RCB XX Cam, and possibly also the hot EHe HD 124448.

In Figure 15, the stars' initial F abundance is assumed to correspond to [F/Fe] = 0 over the range $\log \epsilon(\mathrm{Fe})$ from about 7.5 to 5.0, with the trend starting with a solar F abundance of $\log \epsilon(\mathrm{F}) = 4.4$ at $\log \epsilon(\mathrm{Fe}) = 7.5$ (see below). A star's Fe abundance is assumed to be its initial Fe abundance as an H-normal star. Relative to the assumed F–Fe trend, the typical F overabundance at the solar Fe abundance is 500, and this increases to nearly 2000 for the most metal-poor of the H-deficient stars, namely, the minority RCBs and the cool EHe FQ Aqr. This is an extraordinary overabundance for any element in any star! The common F overabundance among EHe and RCB stars indicates that, as long suspected, these H-deficient stars are probably closely related. (Fluorine abundances have not been measured for HdC stars.) In sharp contrast, the H-deficient spectroscopic binary KS Per has an upper limit to the F abundance consistent with its initial abundance (Pandey 2006), confirming expectations that massive hot binaries like KS Per have an entirely different evolutionary history compared with the EHes and their relatives.

Initial abundances for interpretations of F abundances in EHe and RCB stars are based on the solar abundance and abundances in red giants in the Galactic disk. Solar determinations of the F abundance are determined from infrared lines of HF in sunspot spectra: Maiorca et al. (2014) report a solar F abundance of $\log \epsilon(\mathrm{F}) = 4.40 \pm 0.25$, in fine agreement with the abundance of 4.42 ± 0.06 obtained from meteorites (Lodders et al. 2009). F abundance measurements from HF lines in the spectra of red giants in the Galaxy suggest that [F/Fe] $\simeq 0.0$ over the [Fe/H] interval 0 to -1.5 spanning the interval covered by the EHe and RCB stars (Li et al. 2013;

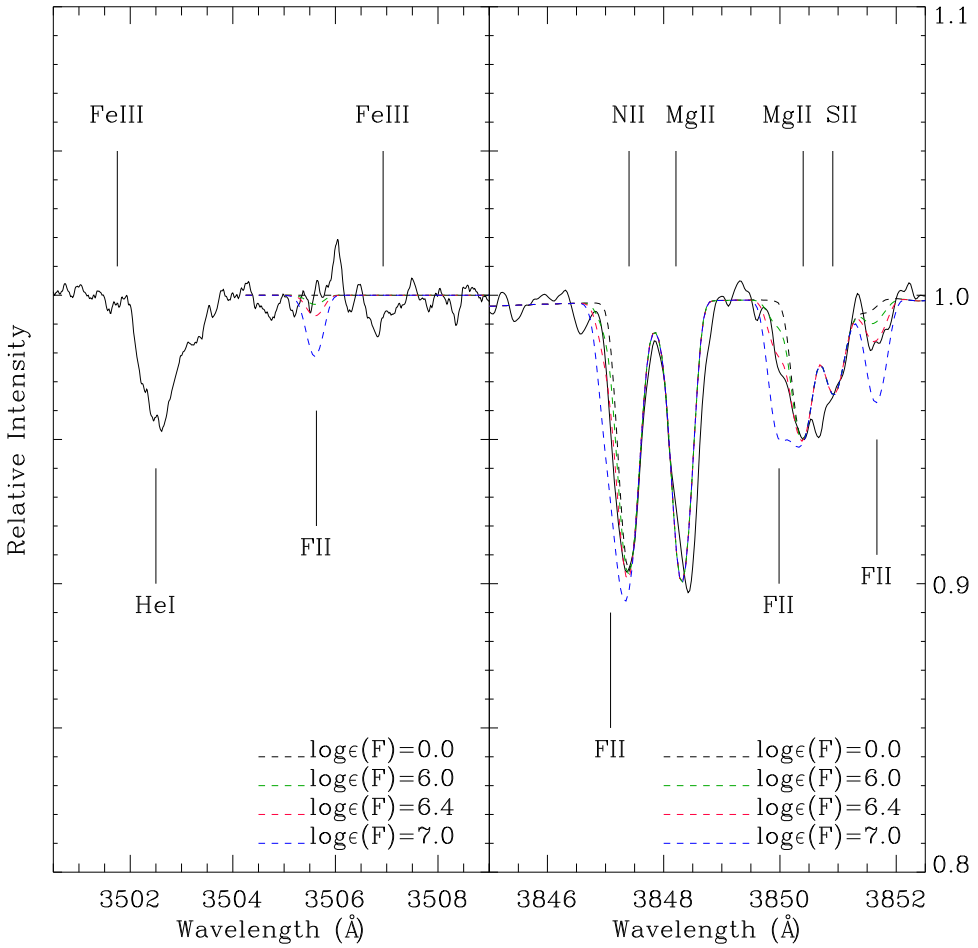

Figure 9. Observed F II in 3500 Å and 3850 Å of BD +10° 2179 (solid line) with key lines marked. Synthetic spectra are shown for four fluorine abundances.

Nault & Pilachowski 2013; Jönsson et al. 2014, 2017; Maiorca et al. 2014; Guerço et al. 2019). Current uncertainty in the F versus Fe relation in Galactic normal stars should not affect the comparison of compositions of EHe, RCB, and HdC stars with theoretical evolutionary scenarios; the F overabundance, in particular, dwarfs the current uncertainty.

4.2. Fluorine and Other Elements

In searching for an explanation for the hot EHes, the cool EHes, and the RCBs, it is helpful to identify the relationships, if any, between the abundances of key elements. No modern analysis for elemental abundances is available for the HdC stars whose spectra are dominated by molecular bands. Consideration of the elemental abundances for RCB stars must recognize that the available analyses of Asplund et al. (2000) identified "the carbon problem." Opacity in the atmosphere of an RCB star appears to be dominated by continuous absorption from excited levels of the neutral carbon atom. Since the many absorption lines of the neutral carbon atom also arise from excited levels, the predicted strength of weak C I lines is almost independent of the principal atmospheric parameters, that is, effective temperature, surface gravity, and the C/He ratio; however, the predicted equivalent widths of weak C I lines is a factor of 0.6 dex stronger than observed. This discrepancy defines the carbon problem, for example, model atmospheres computed for a C abundance of 9.5 (equivalent to a C/He ratio of 1%) return a C abundance of 8.9 from weak C I lines. The carbon problem's implications for abundances and abundance ratios are discussed but not resolved in an extensive investigation of possible solutions by Asplund et al. (2000). Although some proposed resolutions of the carbon problem should have minimal effect on elemental abundances and particularly on abundance ratios, abundances for RCB stars should be used with reservation in effecting comparisons with compositions of EHe stars. EHe stars are not subject to a carbon problem. (Abundances for RCBs are used in Figure 15 where it is clear that the F and Fe abundances of EHe and RCB stars provide overlapping distributions; the Fe and F abundances for RCB stars are not both overestimated by 0.6 dex.)

The likely relationship between F abundances and abundances of C, N, O, and Ne in EHes are shown in Figure 16. Abundances for the RCB stars generally confirm results for the EHes. In the case of C, the spectroscopic C abundances (primarily from Asplund et al. 2000) are systematically 0.6 dex in the mean lower than for the EHes because of the carbon problem. For N, the N abundances from Asplund et al. (2000) and Hema et al. (2017), and the F abundances from Pandey et al. (2008) and Hema et al. (2017) for the RCBs, overlap well with the abundance spread provided by the EHes. For the EHes, the O–F relation may suggest a positive correlation with the RCB stars possibly superimposed on this correlation but lacking stars with the extreme O (>9.1) abundances. Neon abundances are available from LTE analysis of Ne I lines for four RCBs—Y Mus and V3795 Sgr reported by Asplund et al. (2000) and V532 Oph and ASAS−RCB−8 reported by Hema et al. (2017)—but the F

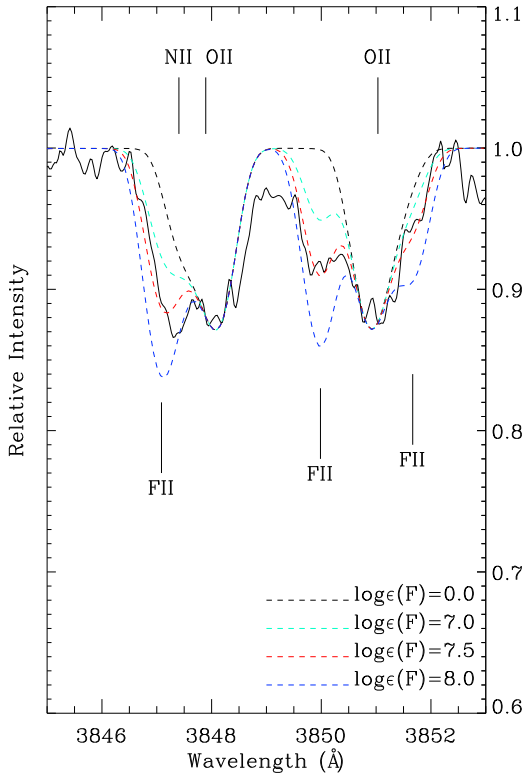

Figure 10. Observed F II in 3850 Å of V1920 Cyg (solid line) with key lines marked. Synthetic spectra are shown for four fluorine abundances.

abundance has been reported only for three : V3795 Sgr (Pandey et al. 2008) and V532 Oph and ASAS−RCB−8 (Hema et al. 2017). The minority RCB V3795 Sgr with the reported Ne abundance falls among the (Ne, F) abundances for hot EHes, but an anticipated non-LTE reduction of about 0.7 dex to the Ne abundance would suggest V3795 Sgr is Ne poor for its F abundance, whereas for the two majority RCBs V532 Oph and ASAS−RCB−8, the non-LTE reduction of 0.7 dex directly places them in (Ne, F) the distribution of hot EHes. LTE neon abundances from Ne I lines are available for five cool EHes (Pandey et al. 2001; Pandey & Reddy 2006) and are compared with fluorine in Figure 16. Except for the cool EHe FQ Aqr, the neon abundances with respect to fluorine for the cool EHes appear systematically higher than (Ne, F) abundances traced by the hot EHes. Clearly, the anticipated non-LTE correction of 0.7 dex will place them with the hot EHes. In addition, the same non-LTE correction on FQ Aqr would suggest that it is Ne poor for its F abundance just like the minority RCB V3795 Sgr.

Independently of the F abundances, relations between the N–Ne–Fe abundances provide clues to the stars' nucleosynthetic history (Figure 17). H burning by the CN cycle increases the N abundance at the expense of C, and the ON cycle provides additional N at the expense of O. In predicting the N abundance from CNO cycling, initial C and N abundances are assumed to follow the relation [C/Fe] = [N/Fe] = 0. Initial O abundances are taken from Ryde & Lambert's (2004) [α/Fe] versus [Fe/H] relation for disk stars with O treated as a typical αelement. Nitrogen is supposed here to be the dominant product of CNO cycling.

Nitrogen abundances as a function of Fe abundances are shown in Figure 17 for the cool and hot EHes against three possible relations: (1) the initial N versus Fe relation, (2) the N abundance versus Fe relation expected if the N abundances arise from the sum of the initial C and N abundances, and (3) the N abundances resulting from the sum of the initial C, N, and O abundances. With the clear exception of the C-poor hot EHe HD 144941, the N and Fe abundances are distributed along line (3), indicating that N is a product of severe CNO cycling in an H-rich region. Two hot EHe stars appear closer to the CN cycling than to the CNO cycling prediction. With the single exception of the C-poor HD 144941, the atmosphere of a hot EHe star appears severely contaminated with material exposed to CNO cycling or possibly in two stars exposed to CN cycling.

LTE nitrogen abundances for cool EHes (Pandey et al. 2001; Pandey & Reddy 2006) obtained from both the N I and N II lines track the N versus Fe trend defined by the majority of the hot EHes from N II lines corrected for non-LTE effects. Nitrogen abundances for RCB stars (Asplund et al. 2000; Hema et al. 2017) from N I lines but not corrected for non-LTE effects provide N abundances higher than those in the cool and hot EHe stars. This offset arises partially from the lack of a correction for non-LTE effects for the RCB stars and mainly is a symptom related to the carbon problem. Correction for non-LTE effects may lower the RCBs' N abundances. In summary, the majority of the H-deficient stars in the RCB-EHe sequence have an N abundance indicative of severe CNO cycling, with the N abundance equaling the initial sum of the C, N, and O abundances for a star's Fe abundance.

Neon is severely overabundant in EHes. Figure 17 (bottom panel) shows the Ne abundances for the hot EHes (Pandey & Lambert 2011; Pandey et al. 2014; Pandey & Lambert 2017), where results come from Ne I lines in all stars and Ne II lines in the few hottest stars. The abundance analysis included non-LTE effects, which were substantial for Ne I lines but small for Ne II lines. When lines from the neutral atom and the singly charged ion were both available, the Ne abundance estimates after non-LTE corrections were in good agreement. See Table 2 of Pandey & Lambert (2011).

As discussed earlier, neon abundances from Ne I lines are available for five cool EHes (Pandey et al. 2001; Pandey & Reddy 2006) and four RCBs (Asplund et al. 2000; Hema et al. 2017). Ne abundances for the cool EHes are clearly systematically higher than for the hot EHes, for example, LS IV -14^{o} 109 has a Ne abundance of 9.4 for a Fe abundance of 6.9 (Figure 17). Such a systematic offset from abundances for the hot EHes is likely due to neglect of the non-LTE effects on the Ne I lines. For the RCBs, Ne with its LTE abundance from Ne I lines falls in Figure 17 slightly above the upper boundary of the points from the hot EHes. Application of the non-LTE corrections should place the RCBs and cool EHes with the hot EHes. Then a majority of hot and cool EHes and the RCBs have a Ne abundance corresponding closely to the sum of the initial C+N+O+Ne abundances.

The upper bound for the Ne versus Fe relation is here set by the condition that the Ne abundance is the sum of the initial C +N+O+Ne abundances, which differs only slightly from the C +N+O sum used in the N versus Fe panel. Initial Ne abundances are again taken from Ryde & Lambert (2004)'s [α/Fe] versus [Fe/H] relation for disk and halo stars. Identification of Ne abundances with this sum implies that material has been exposed to temperatures beyond those generally required for H burning, and the product ^{14}N has been processed by successive αcaptures to ^{22}Ne seemingly with near 100% efficiency. The majority of stars in the (Ne, Fe) panel fall along the (C+N+O+Ne) limit. Among the hot EHes,

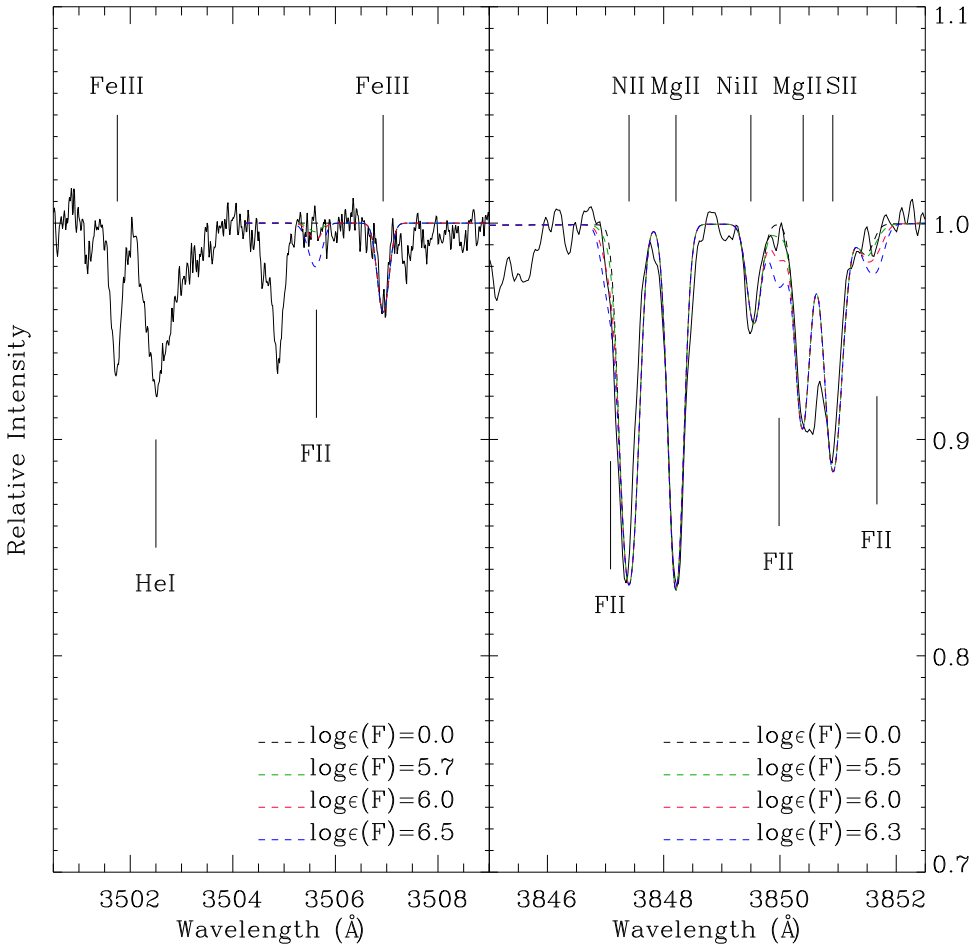

Figure 11. Observed F II in 3500 Å and 3850 Å of HD 124448 (solid line) with key lines marked. Synthetic spectra are shown for four fluorine abundances.

HD 124448 and PV Tel and possibly also the C-poor and Fe-poor HD 144941 display a Ne abundance consistent with the star's initial abundance. HD 124448 and PV Tel have N abundances indicating conversion of initial C+N+O to N by H burning, but both appear to have avoided production of Ne by αcaptures. For V652 Her, the other C-poor hot EHe, the lower Ne abundance implies either less than complete burning of the ^{14}N from CNO cycling to ^{22}Ne and/or partial destruction of the ^{22}Ne by αcaptures. Note that only for four stars, two hot EHes, HD 124448 and PV Tel, and two C-poor hot EHes, V652 Her and HD 144941, where the observed Ne is significantly lower than the initial C+N+O+Ne limit, F II detections are absent, and hence, only the upper limits to the fluorine abundance are placed.

With the single exception of HD 144941, the C-poor EHe, the N abundances of the EHe and RCB stars suggest an atmosphere dominated by gas seriously exposed to H burning such that the initial C, N, and O expected from the Fe abundance have been converted to N through the CNO cycles. The measured Ne abundances of the majority of the hot EHes and the inferred (that is, observed non-LTE corrected) Ne abundances for the cool EHes and RCBs indicate that the Ne as ^{22}Ne was most likely produced with near 100% efficiency by αcaptures from the N in gas previously heavily exposed to H burning. These episodes of H burning and (partial) He burning cannot have occurred in the same gas: Ne synthesis destroys the N, and, in addition, all Ne-rich stars have abundant O. This juxtaposition of abundant N and Ne may point to distinct regions of nucleosynthesis and, perhaps, to a history as a binary system.

Heavy elements offer another signature of nucleosynthesis, namely, the *s*-process. Asplund et al. (2000) noted the overabundance of *s*-process elements in some RCB stars. Overabundances of Zr are found for some hot EHes but in so few stars that a dependence of F on the *s*-process cannot be determined (Table 5). To the hot EHe sample, we add RCB Zr abundances from Asplund et al. (2000) and Hema et al. (2017). Zr for a sample of cool and hot EHes are from Pandey et al. (2006)'s analysis of *Hubble Space Telescope* ultraviolet spectra, and Zr for other cool EHes are from Pandey et al. (2001) and Pandey & Reddy (2006). The full sample with both F and Zr abundances is shown in Figure 18. Severe *s*-process enrichment is certainly present among these H-deficient stars: [Zr/Fe] can exceed +2, but there are also stars lacking in detectable enrichment (i.e., [Zr/Fe] = 0). There is no obvious correlation between the F abundance and [Zr/Fe].

5. Double White Dwarf Mergers and the Fluorine Abundance

Until recently, two scenarios were in competition to explain the sequence EHe—RCB—HdC: the DD and the FF model.

In the FF model, a late or final He shell flash occurs in a post-AGB star, a star on the white dwarf cooling track, and converts the star to a H-poor cool luminous star (i.e., an HdC or RCB star), which then evolves back at about constant luminosity (i.e., as an EHe star) to the white dwarf cooling track (Iben et al. 1983; Herwig 2001). Nucleosynthesis

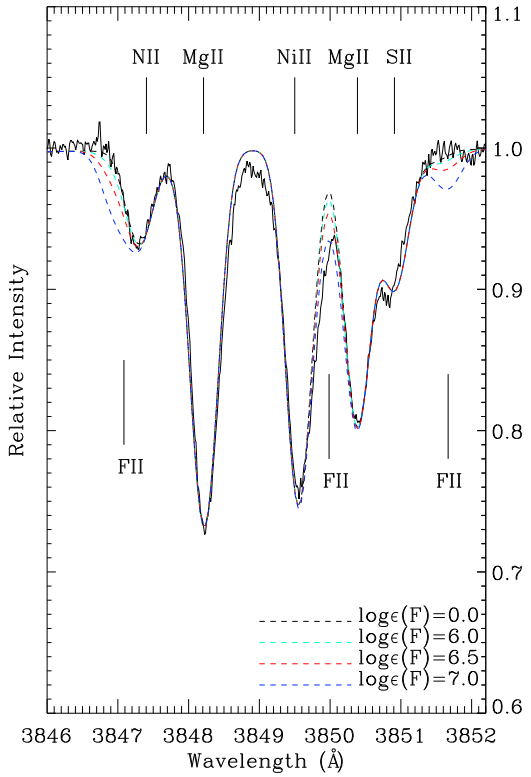

Figure 12. Observed F II in 3850 Å of PV Tel (solid line) with key lines marked. Synthetic spectra are shown for four fluorine abundances.

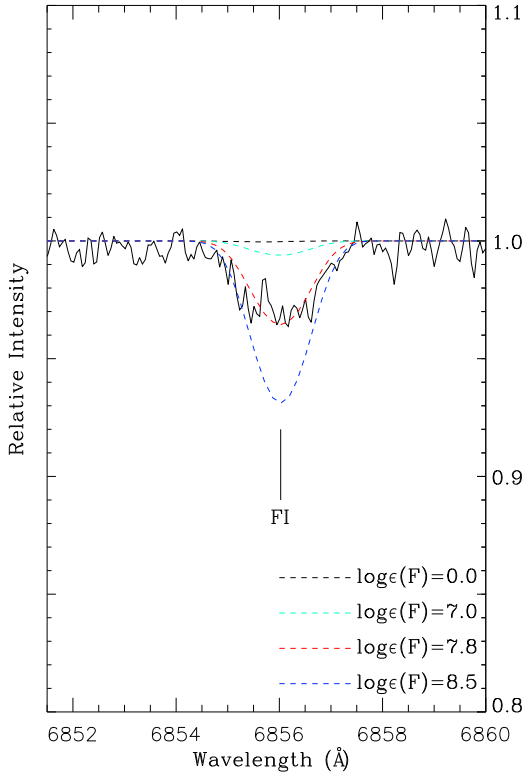

Figure 13. Observed F I in 6856 Å of V1920 Cyg (solid line) with key lines marked. Synthetic spectra are shown for four fluorine abundances.

occuring during and following the He shell flash shows that a H-poor supergiant may result with features of the composition characteristic of EHe, RCB, and HdC stars, but it has proven

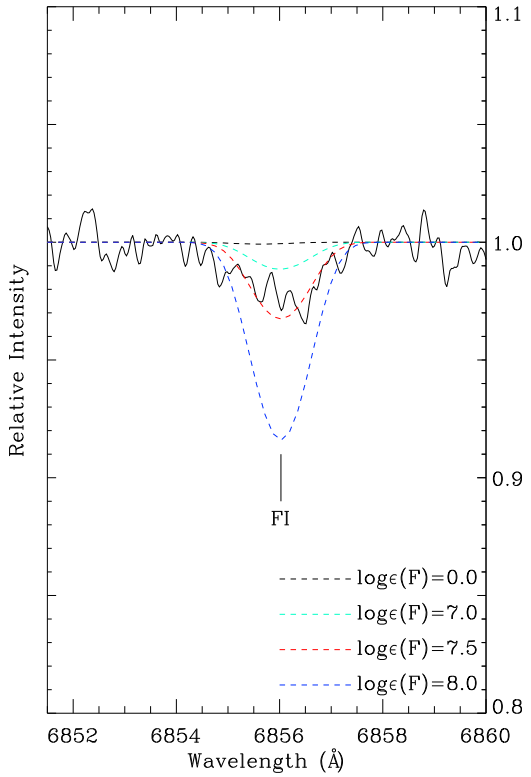

Figure 14. Observed F I in 6856 Å of LSE 78 (solid line) with key lines marked. Synthetic spectra are shown for four fluorine abundances.

difficult to account for the key features, namely, their low $^{16}O/^{18}O$ ratios and their remarkable F overabundances (Pandey 2006; Clayton et al. 2007; Pandey et al. 2008; Hema et al. 2017). The FF model may yet be shown to account for other kinds of H-poor stars (Pandey & Lambert 2011) such as V4334 Sgr (Sakurai's object; Pandey et al. 2008).

In the DD scenario, two white dwarfs merge. In the more favored version of the DD scenario, a He white dwarf is consumed by a more massive C–O white dwarf. In the less favored version, two He white dwarfs merge. Population synthesis shows that CO+He white dwarf binaries are much more likely than He+He white dwarf binaries. Neither version can account for the exceptional ^{18}O abundances in HdC and RCBs and/or the extraordinary F abundances in RCBs and EHes without episodes of nucleosynthesis accompanying the immediate phase of the merger and/or the postmerger phase. Clearly, the final compositions of the resulting single H-deficient stars are likely to depend on the type of the merger, CO+He or He+He, and on details of the stars (masses, compositions, etc.) comprising the close white dwarf binary that by loss of gravitational energy merges. A merger results in a matter of minutes in a complex system comprising the core of the more massive white dwarf (i.e., the C–O white dwarf in the C–O+He system) surrounded by a very hot corona (wonderfully dubbed "the shell of fire") inside a rapidly rotating disk. The disrupted less massive white dwarf is the principal contributor to the corona, which may also receive mass from the more massive white dwarf. The less massive white dwarf is the principal contributor to the disk from which He-rich material is accreted by the central star on a slow timescale, say 10^4–10^5 yr. After the central star has accreted sufficient material, He shell burning commences and the star's envelope expands to become a cool supergiant, that is, an RCB or an HdC supergiant. The

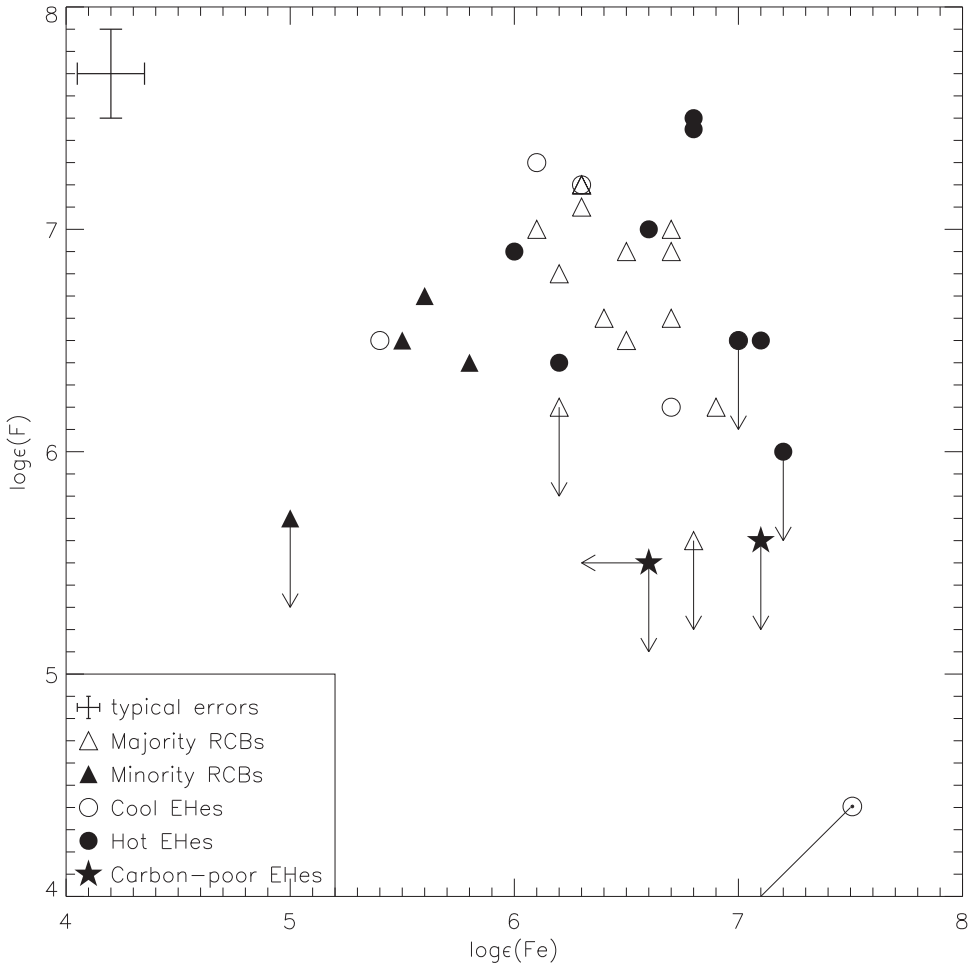

Figure 15. logϵ(F) vs. logϵ(Fe) for hot EHes, cool EHes, and RCBs. The symbols representing different groups of stars are shown. The circled dot symbol represents the Sun, and the solid line represents the locus of the solar F/Fe ratio.

supergiant's surface composition is determined by the compositions of the merging white dwarfs, the nucleosynthesis occurring in the initial brief coronal phase of the merger and in the supergiant's He shell-burning phase and by the (complex) physics of the whole merger process. Simulations of the merger and postmerger phases have yet to reach the finality to which the commendation "ab initio" may be attached appropriately.

Our focus here is on published calculations of the DD scenario and their ability to match the observed F abundances of these H-deficient stars and, in general, their overall compositions including the remarkably low $^{16}O/^{18}O$ ratios of HdC and RCB stars (Clayton et al. 2007), whose discovery has stimulated much of the theoretical work on these H-deficient stars. For detailed descriptions of the various theoretical calculations one should consult the original papers. Our principal comparisons are with predictions for CO+He white dwarf mergers provided by Lauer et al. (2019) and by Menon et al. (2013) and Menon et al. (2019). Lauer et al. (2019) provide commentary on other calculations of CO+He white dwarf mergers including Longland et al. (2011), Zhang et al. (2014), and Menon et al. (2013) and Menon et al. (2019).

Lauer et al. (2019) report on modeling of CO+He white dwarf mergers for stars initially of solar composition, that is, [Fe] = 0. Most simulations consider a 0.55 $M_{\odot}$ CO white dwarf leading to a postmerger mass of 0.8 $M_{\odot}$. Predicted abundances for their principal product of a merger labeled A1 are summarized in their Figure 6. Model A1 deserves a fair pass against the observations of the $^{16}O/^{18}O$ ratios and the F abundances of HdC, RCB, and EHe stars extrapolated to [Fe] $\sim$ 0. Fluorine as synthesized in the hot corona is about a factor of 3 less than observed. Observed C abundances are slightly underpredicted. Model A1 also underpredicts the N abundance. Neon, as ^{22}Ne, is predicted to be overabundant at the surface, but quantitative estimates are not provided. For other elements, Na to Ti, observed and predicted abundances match quite well. Lithium production occurs in the A1 model, providing a Li abundance at about the level seen in those few RCBs exhibiting Li.

Menon et al. in their 2013 paper considered four mergers for stars with initial [Fe] = 0 and in their 2019 paper extended their study to merging stars with [Fe] = −1.4 and thus spanned the [Fe] range of the observed EHe and RCB stars. Predicted surface compositions for [Fe] = 0 and −1.4 with regards to $^{16}O/^{18}O$ and F match observations quite well. The predicted F enrichment reproduces the observed F abundances. Menon et al. (2013) note that one source of F is in the He-burning shell of the postmerger star where ^{13}C $(\alpha, n)^{16}O$ serves as a neutron source and ^{14}N is both a neutron poison and an F source: $^{14}N(n, p)^{14}C(p, \gamma)^{15}N(\alpha, \gamma)^{19}F$. Predicted C and O abundances exceed observations, an issue discussed by Menon et al. (2019). Note that the reported observed [O] abundances in Figure 5 of Menon et al. (2019) are overestimated by about 0.7 dex. Predicted N abundances match observations quite well. In the hot corona, neutrons are released

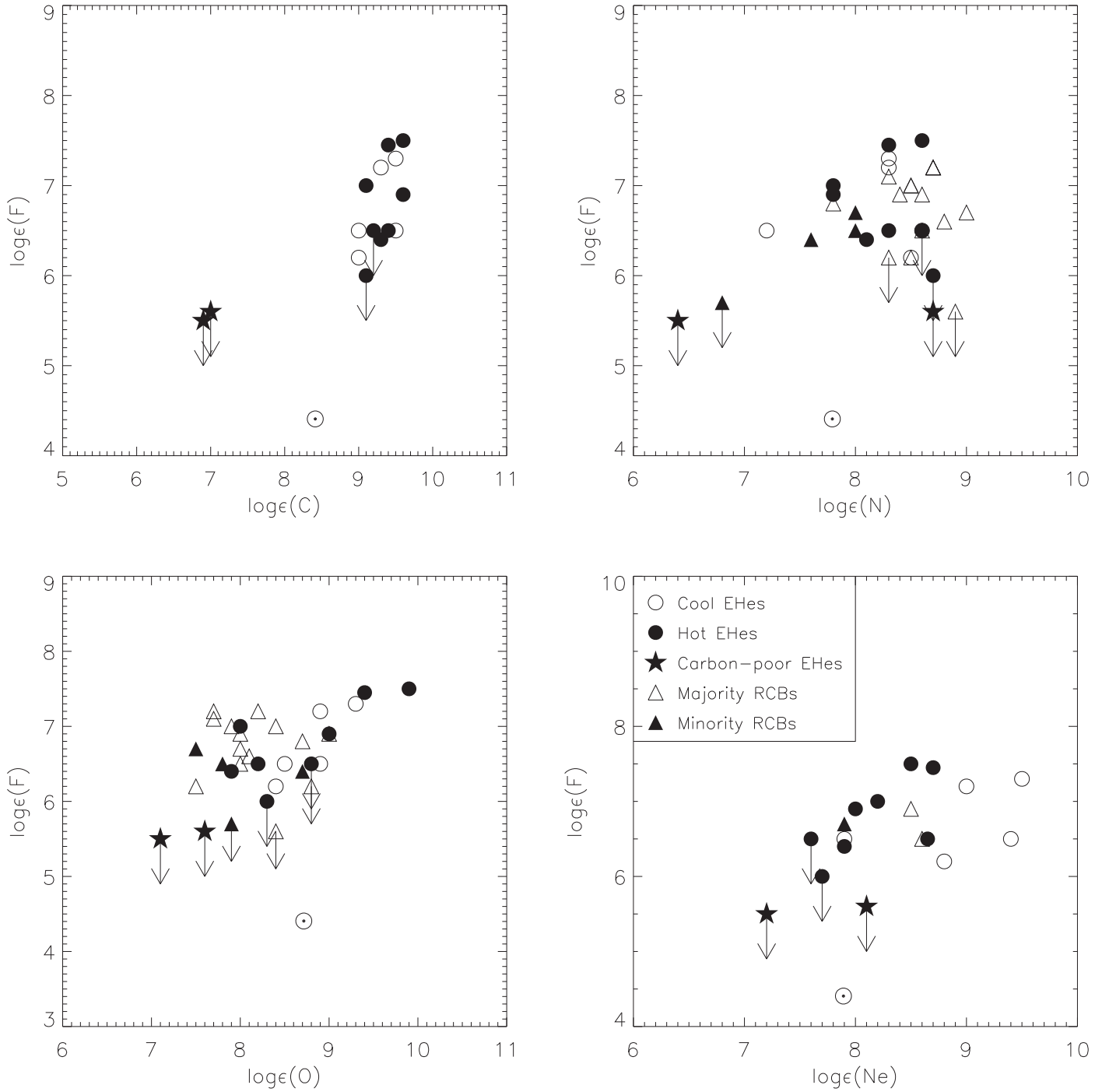

Figure 16. Observed logϵ(F) vs. logϵ(X) for EHes and RCBs from where X = C, N, O, and Ne, respectively. The encircled dot symbol represents the Sun.

in some models, and enrichment of *s*-process heavy elements is predicted. Observed *s*-process enhancements are found in some EHes and RCBs; see Figure 18. Predictions for Zr roughly match the observed maximum [Zr/Fe] for the models that release neutrons. The range of light *s*-process enhancements predicted approximately matches the range of [Zr/Fe] shown in Figure 18. However, one simulation experiencing severe Zr enrichment also predicted substantial enrichment of heavy *s*-procss elements such as Ba and La, that is, [Ba/Fe] = 4, which is not observed. Minor changes to the Na and Al abundances were predicted primarily as a result of proton captures. Explicit predictions of the surface Ne abundances were not given, but appreciable synthesis of neon as ^{22}Ne occurs in these models. In all published simulations the abundant isotope of neon is ^{22}Ne not the commonly abundant ^{20}Ne isotope.[7]

[7] Although the isotopic wavelength shifts of Ne I and Ne II lines may be measurable with precision in the laboratory, differentiation between the two Ne isotopes in a spectrum of an EHe will not be a trivial matter. A catalog of isotopic shifts between ^{20}Ne and ^{22}Ne for Ne I lines is given by Ohayon et al. (2019) and for Ne II lines by Öberg (2007). The maximum shift for our selection of lines for Ne I is about 1.5 km s^{-1} and for Ne II is about 2.5 km s^{-1}. With a careful selection of comparison lines around the Ne I and Ne II lines it may be possible to show that the stellar Ne lines share the radial velocity of the star provided that the ^{22}Ne wavelengths are adopted. However, the stellar lines have an FWHM of about 10–30 km s^{-1}, and line widths and velocities may differ according to their depth of formation in the stellar atmosphere.

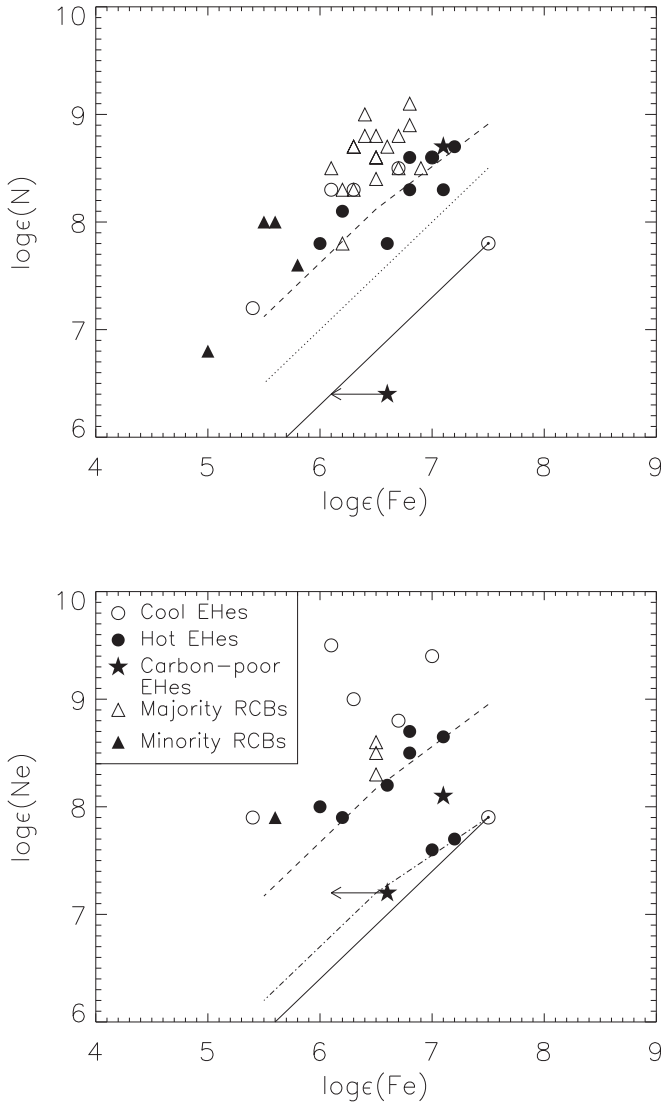

Figure 17. Observed logϵ(N) and logϵ(Ne) vs. logϵ(Fe) for EHes and RCBs. The encircled dot symbol in each plot corresponds to the solar value, with the solid line giving the locus of the solar ratios N/Fe and Ne/Fe, respectively. The dashed line in the plot of logϵ(N) vs. logϵ(Fe) is the predicted nitrogen after full conversion of initial C, N, and O to nitrogen in the CNO cycle where initial O is determined from the relation of [α/Fe] vs. [Fe/H] for normal disk and halo stars given by Ryde & Lambert (2004). The dotted line in the same plot is the predicted nitrogen due to conversion of inital C and N to nitrogen in the CN cycle. In the plot of logϵ(Ne) vs. logϵ(Fe), the dashed–dotted line gives the locus of initial neon values taken from the relation of [α/Fe] vs. [Fe/H] for normal disk and halo stars (Ryde & Lambert 2004). In the same figure the dashed line is the locus giving the sum of initial C, N, O, and Ne.

Considering the complexity of the physics and the variety of initial conditions for the two white dwarfs in the CO+He merger, it seems fair to conclude that the DD scenario with CO +He white dwarf mergers as presently simulated provides an adequate account of the two principal abundance anomalies of RCB and EHe stars, namely, the $^{16}O/^{18}O$ ratios and F abundances and the C, N, O and Ne abundances without introducing other anomalies that are not matched by observations. It remains to examine whether the alternative possibility of He+He white dwarf mergers may also account for the compositions of some RCB and EHe stars. Noting that Zhang & Jeffery (2012b) indicate that production of RCB and EHe stars via the He+He channel may be 14–70 times smaller than

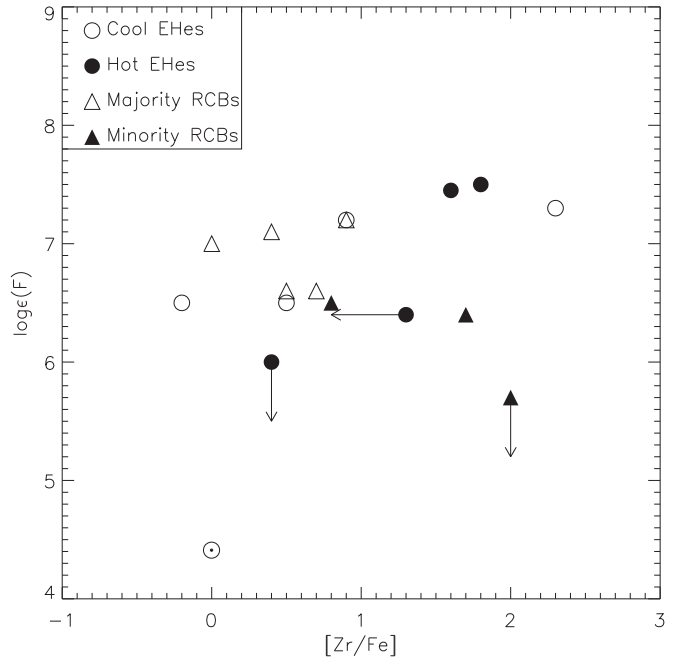

Figure 18. Observed logϵ(F) with [Zr/Fe] for EHes and RCBs. The encircled dot symbol represents the Sun.

from the CO+He channel, H-deficient stars created by the He+He channel may be the exception among the observed population of RCB and EHe stars.

Simulations of He+He white dwarf mergers as an explanation for H-deficient stars appear to be limited to those by Zhang & Jeffery (2012a, 2012b) who explored restricted ranges for the many parameters entering into the simulations. Zhang & Jeffery (2012b) considered the merger of two 0.4 $M_{\odot}$ He white dwarfs for four metallicities from $Z = 0.02$ to $Z = 0.0001$. Predicted surface abundances of the resulting RCB and EHe stars were "in partial agreement" with the observed abundances. In particular, the models showed "a strong overabundance of F [relative to the initial F abundance]" but not enough to fully agree with the observational data. The disagreement was a factor of 100 at [Fe] $= -2$ decreasing to a factor of about 20 at [Fe] $= -1$. In these mergers, the F is synthesized by ^{14}N (α, γ)^{18} F (p, α)^{15} O (α, γ)^{19} Ne (β^{+})^{19} F. Enrichment of ^{18}O may be underpredicted too. Minor disagreements between prediction and observation are found for C, N, O, and Ne. The RCBs and EHes are predicted to be C rich not C poor at all Z. Lithium, which is observed in a few RCBs, is not predicted to be present in the merged star.

In Zhang & Jeffery (2012a), four models of equal-mass pairs of He white dwarfs were followed: total masses considered were 0.5, 0.6, 0.7, and 0.8 $M_{\odot}$ for initial compositions $Z =$ 0.02 and 0.001. An aim of the calculations was to examine the effect of "slow" mergers (the accreted star forms a disk around the accreting star from which gas is accreted at $10^{-5} M_{\odot}$ yr^{-1}), "fast" mergers corresponding to an accretion rate of $10^{4} M_{\odot}$ yr^{-1} for the remaining white dwarf, and "composite" mergers in which about 50% of the donor star's mass is accreted rapidly and the remainder forms a disk from which gas is accreted at the "slow" rate. Predicted compositions for the merged 0.5–0.8 $M_{\odot}$ stars were given for just ^{12}C, ^{14}N, ^{18}O, and ^{22}Ne, and comparisons with observed compositions were made with helium-rich hot subdwarfs and not RCB and EHe stars. While F was not reported for these simulations, their relevance

to our determinations of F abundances may be the conclusion that composite mergers from these equal-mass white dwarf pairs show an appreciable C underabundance for combined masses below about 0.6 $M_{\odot}$ with little change of N across the mass range of 0.5–0.8 $M_{\odot}$, and thus the N/C ratio is predicted to increase as the mass decreases below about 0.65 $M_{\odot}$. This prediction, as Zhang & Jeffery (2012a) note, likely accounts for the two classes of He-sdO stars: the N rich with $N/C \gg 20$ and the C rich with $N/C \leqslant 0.1$. The same prediction may provide the latitude to account for the C-poor V652 Her and HD 144941 with their different N/C ratios, but their masses would have to be between 0.6 and 0.7 $M_{\odot}$. One might also put the RCB XX Cam in this narrow range.

6. Concluding Remarks

With observed determinations of the compositions of the H-deficient stars—HdC, RCB, and EHe—and theoretical simulations of the merger of a CO white dwarf with a He white dwarf—the DD scenario—the many decades mystery surrounding compositions of these stars has been resolved. In particular, the large F overabundances for hot EHe stars derived in this paper and compatible with F abundances obtained previously for cool EHe and RCB stars are thanks to detailed simulations, for example, Menon et al. (2013, 2019) and Lauer et al. (2019), of the DD scenario known to be quantitatively expected. Indeed, the simulations account well for the observed chemical compositions of the HdC, RCB, and EHe sequence including the remarkably low $^{16}O/^{18}O$ ratio (Clayton et al. 2007), which with the F overabundances are the outstanding abundance anomalies of these H-deficient stars.

In the future, observers will be challenged to refine the determinations of chemical composition by not only obtaining more accurate analyses for elements previously studied but by searching for the small abundance changes in the elements Na to Zn and in the *s*-process elements predicted by the available quantitative studies of white dwarf mergers. A major lacuna in the abundance analyses concerns the non-LTE formation of the F I and F II lines, but this gap in quantitative knowledge does not affect the conclusion that the F overabundance in these H-deficient stars is enormous and can be only slightly affected by inclusion of non-LTE effects.

On the theoretical side, exploration of the DD scenario should continue. Predicted abundances of light elements should be tested more thoroughly than hitherto against observed abundance ratios. For example, the puzzles represented in Figure 17 deserve close scrutiny: How can N and Ne both have the abundance implied by total conversion of initial C, N, and O? Perhaps, the range of chemical compositions of HdC, RCB, and EHe stars may be used to set constraints on the boundary conditions for participants in a merger and in the physical conditions during and following the merger with the ultimate hope of achieving ab initio predictions for the family of H-deficient stars.

A.B. and G.P. thank the staff at the IAO, Hanle, and at the remote control station at CREST, Bengaluru, for their assistance with observations. We thank Falk Herwig for exchanges about Ne abundances in white dwarf mergers.

ORCID iDs

Anirban Bhowmick https://orcid.org/0000-0001-6731-4651
Gajendra Pandey https://orcid.org/0000-0001-5812-1516
David L. Lambert https://orcid.org/0000-0003-1814-3379

References

Asplund, M., Gustafsson, B., Lambert, D. L., et al. 2000, A&A, 353, 287
Clayton, G. C., Geballe, T. R., Herwig, F., Fryer, C., & Asplund, M. 2007, ApJ, 662, 1220
Guerço, R., Cunha, K., Smith, V. V., et al. 2019, ApJ, 876, 43
Hema, B. P., Pandey, G., Kamath, D., et al. 2017, PASP, 129, 104202
Herwig, F. 2001, Ap&SS, 275, 15
Hubeny, I., Lanz, T., & Jeffery, C. 1994, Newsletter on Analysis of Astronomical Spectra (TLUSTY and SYNSPEC: a User's Guide), Vol. 20, (St. Andrews: St. Andrews Univ.)
Iben, I., Jr., Kaler, J. B., Truran, J. W., & Renzini, A. 1983, ApJ, 264, 605
Iben, I., Jr., & Tutukov, A. V. 1984, ApJS, 54, 335
Jeffery, C. S. 2017, MNRAS, 470, 3557
Jeffery, C. S., Heber, U., Hill, P. W., et al. 1996, in ASP Conf. Ser. 96, Hydrogen Deficient Stars, ed. C. S. Jeffery & U. Heber (San Francisco, CA: ASP), 471
Jönsson, H., Ryde, N., Harper, G. M., et al. 2014, ApJL, 789, L41
Jönsson, H., Ryde, N., Spitoni, E., et al. 2017, ApJ, 835, 50
Lauer, A., Chatzopoulos, E., Clayton, G. C., Frank, J., & Marcello, D. C. 2019, MNRAS, 488, 438
Li, H. N., Ludwig, H.-G., Caffau, E., et al. 2013, ApJ, 765, 51
Lodders, K., Palme, H., & Gail, H.-P. 2009, LanB, 4, 712
Longland, R., Lorén-Aguilar, P., José, J., et al. 2011, ApJL, 737, L34
Maiorca, E., Uitenbroek, H., Uttenthaler, S., et al. 2014, ApJ, 788, 149
Menon, A., Herwig, F., Denissenkov, P. A., et al. 2013, ApJ, 772, 59
Menon, A., Karakas, A. I., Lugaro, M., Doherty, C. L., & Ritter, C. 2019, MNRAS, 482, 2320
Moore, C. E. 1972, NSRDS-NBS, 40, 1
Moore, C. E. 1993, Tables of Spectra of Hydrogen, Carbon, Nitrogen, and Oxygen Atoms and Ions (Boca Raton, FL: CRC Press)
Nault, K. A., & Pilachowski, C. A. 2013, AJ, 146, 153
Öberg, K. J. 2007, EPJD, 41, 25
Ohayon, B., Rahangdale, H., Geddes, A. J., et al. 2019, PhRvA, 99, 042503
Pandey, G. 2006, ApJL, 648, L143
Pandey, G., Kameswara Rao, N., Jeffery, C. S., & Lambert, D. L. 2014, ApJ, 793, 76
Pandey, G., Kameswara Rao, N., Lambert, D. L., Jeffery, C. S., & Asplund, M. 2001, MNRAS, 324, 937
Pandey, G., & Lambert, D. L. 2011, ApJ, 727, 122
Pandey, G., & Lambert, D. L. 2017, ApJ, 847, 127
Pandey, G., Lambert, D. L., Jeffery, C. S., & Rao, N. K. 2006, ApJ, 638, 454
Pandey, G., Lambert, D. L., & Kameswara Rao, N. 2008, ApJ, 674, 1068
Pandey, G., & Reddy, B. E. 2006, MNRAS, 369, 1677
Ryde, N., & Lambert, D. L. 2004, A&A, 415, 559
Sriram, S., Kumar, A., Surya, A., et al. 2018, Proc. SPIE, 10702, 107026K
Tull, R. G., MacQueen, P. J., Sneden, C., & Lambert, D. L. 1995, PASP, 107, 251
Webbink, R. F. 1984, ApJ, 277, 355
Wiese, W. L., Fuhr, J. R., & Deters, T. M. 1996, Atomic Transition Probabilities of Carbon, Nitrogen, and Oxygen: A Critical Data Compilation (Washington, D.C.: National Institute of Standards and Technology)
Zhang, X., & Jeffery, C. S. 2012a, MNRAS, 419, 452
Zhang, X., & Jeffery, C. S. 2012b, MNRAS, 426, L81
Zhang, X., Jeffery, C. S., Chen, X., & Han, Z. 2014, MNRAS, 445, 660